Techno-Economic Optimization of Medium Temperature Solar-Driven Subcritical Organic Rankine Cycle

Tryfon C. Roumpedakis * [ID]**, Nikolaos Fostieris, Konstantinos Braimakis** [ID]**, Evropi Monokrousou, Antonios Charalampidis and Sotirios Karellas**

Laboratory of Steam Boilers and Thermal Plants, Department of Thermal Engineering, School of Mechanical Engineering, National Technical University of Athens, 9 Heroon Polytechniou Street, 15780 Zografou, Greece; nfostieris@gmail.com (N.F.); mpraim@central.ntua.gr (K.B.); evropimonokrousou@gmail.com (E.M.); antonishar@mail.ntua.gr (A.C.); sotokar@mail.ntua.gr (S.K.)

* Correspondence: troumpedak@central.ntua.gr; Tel.: +30-2107722720

Abstract: The present work focuses on the techno-economic assessment and multi-objective genetic algorithm optimization of small-scale (40 kW$_{th}$ input), solar Organic Rankine Cycle (ORC) systems driven by medium-to-high temperature (up to 210 °C) parabolic dish (PDC) and trough (PTC) collectors. The ORCs are designed to maximize their nominal thermal efficiency for several natural hydrocarbon working fluids. The optimization variables are the solar field area and storage tank capacity, with the goal of minimizing the levelized cost of produced electricity (LCoE) and maximizing the annual solar conversion efficiency. The lowest LCOE (0.34 €/kWh) was obtained in Athens for a high solar field area and low storage tank capacity. Meanwhile, the maximum annual solar conversion efficiencies (10.5–11%) were obtained in northern cities (e.g., Brussels) at lower solar field locations. While PTCs and PDCs result in similar efficiencies, the use of PTCs is more cost-effective. Among the working fluids, Cyclopentane and Cyclohexane exhibited the best performance, owing to their high critical temperatures. Notably, the systems could be more profitable at higher system sizes, as indicated by the 6% LCoE decrease of the solar ORC in Athens when the nominal heat input was increased to 80 kW$_{th}$.

Keywords: organic Rankine cycle; solar energy; genetic algorithm

1. Introduction

Organic Rankine Cycle (ORC) technology is widely considered for various applications, including geothermal energy [1], biomass [2], waste heat recovery [3] and the production of electricity through the utilization of solar thermal energy, due to its suitability for operation at small power capacities and relatively low temperatures below 300 °C, in which the conventional steam-Rankine cycle is technically infeasible or not cost-effective. Solar ORCs are oriented toward grid-connected or distributed generation (i.e., to cover the electricity demands of isolated industrial consumers or in the context of community mini-grids) [4] as well as desalination [5] and irrigation [6] applications. In contrast to more mature photovoltaics (PV), the key advantage of solar ORCs is their capability for cost-effective thermal energy storage (TES), which comes at a lower cost than electrochemical batteries [7]. The cost-effective energy storage of solar ORCs can also make them more profitable as dispatchable power sources in the renewable energy-dominated landscape. Considering the above, the investigation of their thermodynamic and economic performance becomes increasingly significant.

Up to date, several thermodynamic and techno-economic studies on the simulation and optimization of solar ORCs have only considered their nominal design points. One of the first studies following this approach was conducted by Tchanche et al. [8], who investigated different fluids for low-temperature solar ORCs and highlighted the importance of different evaluation criteria that need to be taken into account during the selection process.

A study of similar scope was carried out by Delgado-Torres and García-Rodríguez [9], who evaluated the on-design performance of low-temperature (<145 °C) solar recuperative ORCs driven by flat plate collectors (FPCs). The authors highlighted the overall superior performance of dry fluids, with isopentane, R245ca, R245fa and isobutane featuring the minimum solar collector areas per produced kW$_e$ of electrical output. A study of similar scope but focusing on a concentrated solar power (CSP) standard and recuperative ORC with a power capacity of 20 kWe was carried out by Ferrara et al. [10]. The authors compared the performance of three fluids: R134a, R245fa and acetone. For the latter, a cycle efficiency of 20% was calculated (recuperative ORC). Finally, the authors suggested that piston expanders are the most suitable expander technology, due to the capability of handling low fluid rates and high-pressure ratios. Other studies follow similar approaches but put more emphasis on novel configurations and components. For example, Shahverdi et al. [11] investigated the installation of an Archimedes screw turbine in the heat transfer loop of a solar ORC driven by parabolic trough collectors (PTCs), considering different working fluids. In this study, two types of absorbers were evaluated, consisting of smooth and corrugated tubes. The best performance in terms of net power as well as cycle (25%) and total efficiency (about 17%) was obtained by R113, while the corrugated tube absorber was superior. Deligant et al. [12] assessed the potential of using a standard radial turbine as an expander in a solar ORC by conducting computational fluid dynamics (CFD) simulations, which indicated that isentropic efficiencies of up to 78% were achievable.

Another topic that is widely investigated is the performance of solar cogeneration (combined heat and power-CHP) and trigeneration (combined cooling heat and power-CCHP) systems including ORCs, which come in different varieties, depending on the employed cooling technology, which can be (among different solutions) a vapor compression cycle (VCC) [13], an absorption chiller [14] an adsorption chiller [15] or an ejector-based cycle [16] in different configurations. Some indicative examples are presented in the following. Jafary et al. [17] investigated a PTC-driven system consisting of two different types of ORCs (recuperative and regenerative) and an absorption chiller. The overall energy and exergy efficiencies of the systems were 93.35% and 12.69% (recuperative) and 80.66% and 6.64% (regenerative system). Khaliq et al. [18] investigated a system including an ORC and a hybrid cooling cycle involving an absorption chiller and an ejector device and examined the influence of different design parameters on the energetic and exergetic performance. In a particular scenario in which isobutane was considered as the ORC working fluid, the overall energy and exergy efficiencies were 65.42% and 13.98%, respectively. Braimakis et al. [19] evaluated the thermodynamic and economic performance of a hybrid solar-biomass trigeneration system based on the combination of an ORC and a VCC. The authors reported ORC thermal efficiencies between 3.7% and 10.05% for different organic fluids and conditions, while the cogeneration efficiency could be as high as 73.5% resulting in a payback period of 12.3 years.

Several studies have considered the off-design operation of solar ORCs, which is of high significance due to the daily and seasonal variability of solar radiation. In these studies, off-design simulation models for the solar collectors, storage tank and ORC equipment components (heat exchangers, expanders, pumps) are developed and interconnected, while different control strategies are defined to determine the operational mode of the system under different solar availability and energy demand scenarios. In this way, the operation of the solar ORC is simulated under variable heat input from the solar collectors (usually considering an hourly time step) and its performance is assessed based on its operation throughout a particular period (daily, seasonal or annual).

Baccioli and Desideri [20] developed a dynamic simulation model of a solar ORC operating with R600a driven by compound solar collectors with a maximum heat transfer fluid (HTF) temperature of 140 °C. A sliding-velocity control strategy was assumed for the ORC, which, according to the authors, could drive the plant without requiring a thermal energy storage system (TES). In another study, Wang et al. [21], implemented a genetic algorithm (GA) based methodology for optimizing recuperative solar ORCs driven by

FPCs under variable solar radiation. The authors concluded that the best daily performance was obtained by working fluid R123, which had a daily energy efficiency of 7.59% at a maximum cycle temperature of 69.84 °C. Freeman et al. [22] investigated the working fluid selection and thermodynamic optimization aspects of a domestic solar ORC for CHP production. The ORC was driven by evacuated tube collectors (ETCs) of a 15 m^2 area, while the temperature of the HTF was varied from 90 °C to 240 °C. When considering a standard, single-stage collector configuration, the authors concluded that the optimal system resulted in an annual work output equal to 955 kWh/year. Furthermore, the authors additionally evaluated a modified configuration that included a two-stage solar collector array which, owing to its improved efficiency, could lead to a 12% increase in the annual work output. In both cases, R245ca was found to be the optimal working fluid. Kutlu et al. [23] investigated the off-design performance of a small-scale solar ORC equipped with a pressurized hot water storage tank and driven by an ETC field of 500 m^2 with a nominal maximum hot water temperature of 110 °C. The power output of the ORC, which operated with R245fa, varied between 4.3 kWe and 11.2 kWe throughout 24 h, while its efficiency ranged from 7.6% to 9.2%. Petrollese and Cocco [24] introduced a thermodynamic and techno-economic optimization approach for large-scale solar recuperative ORCs operating with linear Fresnel collectors (LFCs) of a total area of 8500 m^2, operating with a nominal HTF temperature equal to 275 °C and considering the use of three different working fluids, hexamethyldisiloxane, toluene and n-heptane. The off-design modeling approach was based on the definition of a probability distribution of multiple operating scenarios including different HTF mass flow rates and temperatures as well as ambient temperatures. Among the examined working fluids, toluene led to the lowest levelized cost of electricity (LCoE), which was equal to 122 €2019/MWh$_e$, while also having a cycle efficiency of 19.5%. Casartelli et al. [25] investigated different off-design control strategies for a 5 MW$_e$ solar ORC driven by LFCs featuring maximum HTF temperatures of 390 °C and 310 °C and operating with toluene. Among the two investigated control strategies (sliding pressure and fixed pressure-partial admission at turbine inlet), the second resulted in higher electrical power output and efficiency. Patil et al. [26] carried out a techno-economic performance comparison between a PV (with and without battery storage) and a PTC-driven ORC system having a nominal power capacity of 50 kWe. The authors concluded that while the stand-alone PV (capacity factor 0.27) had the overall lowest LCoE (0.12 USD2018/kWh$_e$) when a higher capacity factor (0.56) was considered, the LCoE of the solar ORC (0.19 USD2018/kWh$_e$) was lower than that of the PV-battery module (0.26 USD2018/kWh$_e$). Li et al. [27] also evaluated the off-design performance of a solar ORC driven by CPCs and highlighted the importance of proper TES sizing to minimize dynamic resonance phenomena.

Most studies on small-scale solar ORCs focus on low- or mid-temperature applications featuring flat plate and evacuated tube collectors with nominal cycle temperatures below 150 °C. As a result, the thermodynamic and techno-economic performance of micro- and small-scale solar ORCs driven by concentrated solar collectors such as parabolic trough and dish collectors, which enable their more efficient operation at higher temperatures, has not been thoroughly evaluated. Furthermore, in most techno-economic studies on solar ORCs, only their on-design performance is assessed, while their off-design operation, which is of high importance considering the intermittent and variable nature of solar energy, is neglected. Finally, in many studies, the optimization of key design variables of solar ORCs is not undertaken, as their goal is only the simulation/evaluation of system performance under different scenarios.

Aiming to address the aforementioned research gaps, the present work aims at the systematic techno-economic optimization of high-temperature solar ORCs driven by PTCs and parabolic dish collectors (PDCs), considering their off-design, annual performance in five European cities, namely Athens, Madrid, Rome, Brussels and Berlin. The selection of these cities was based on their climate classification according to the Köppen-Geiger climate specification [28]. More specifically, since the cities are located in southern and central Europe, they are associated with sufficient annual direct solar irradiation, which

is necessary for the cost-effectiveness of the proposed solar ORC (Table 1). Regarding the southern cities, all of them are characterized by a Mediterranean climate. However, while Rome's climate is standard Mediterranean, Athens and Madrid have hotter and colder semi-arid climates, respectively. Meanwhile, Berlin and Brussels have Marine West Coast climates. The selection of cities with different climate characteristics helps to examine the impact of climate on system performance and profitability. As a matter of fact, Madrid and Athens exhibit the highest annual direct normal irradiance, while the corresponding value for Brussels is almost three times less and slightly lower than in Berlin.

Table 1. Annual direct normal irradiance for a number of European cities.

City	Athens	Madrid	Rome	Brussels
Value (MWh/m^2)	1519.8	1542.3	1204.8	508.9
City	**Berlin**	**Dublin**	**Warsaw**	**Copenhagen**
Value (MWh/m^2)	585.1	577.45	676.5	698.6

The off-design performance of the solar ORC is evaluated with the development and integration of a series of off-design models for all equipment components (solar collectors, thermal energy storage tank, heat exchangers, expander, pump, motor/generator) to accurately simulate their operation under realistic, variable conditions. Furthermore, cost correlations based on literature data and manufacturers' datasheets are used for capital and operational cost estimation. In each case, a GA optimization technique is implemented to determine the optimal solar field area and storage tank capacity with regard to the maximum annual total solar energy conversion efficiency and minimum LCoE of the solar ORCs. GA optimization belongs to the larger class of evolutionary algorithms, which are based on Darwin's theory of evolution [29]. Nowadays, this optimization method is applied with many variations to numerous engineering problems and has been used on several occasions for the thermodynamic and technoeconomic optimization of ORC systems of various configurations and types [30–32].

2. Methods

The layout of the investigated system is illustrated in Figure 1. The HTF is heated in the field of solar collectors and is conveyed to the heat storage tank in the collectors' sub-circuit. Subsequently, depending on the operating mode of the system, the HTF circulates from the storage tank to the ORC evaporator to provide heat to the cycle.
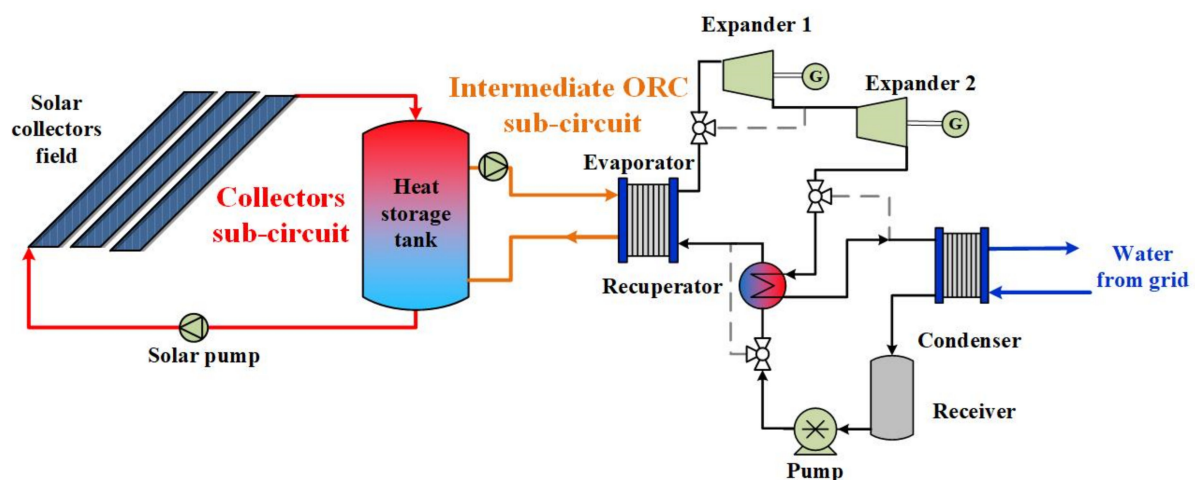

Figure 1. Layout of the investigated solar-driven ORC with a recuperator and two serial expanders.

Depending on the operating conditions, a second expander is considered when the pressure ratio of the cycle is higher than a maximum expansion ratio (to be discussed in more detail in Section 2.3). Meanwhile, a recuperator is added to recover heat from the expanded superheated vapor for preheating the subcooled liquid after the pump (also presented in more detail in Section 2.3). Finally, the working fluid is condensed in a water-cooled condenser.

In the following sections, the models that are used for simulating the operation and the solar-driven ORC subsystem's performance are described in detail.

2.1. Solar Collectors

A medium to high-temperature ORC is investigated; hence, only concentrating collectors are considered. These collectors utilize only the sun's direct radiation; the sunlight is reflected and focused onto a receiver, which absorbs the radiation with a concentration ratio higher than 1, resulting in higher heat flux and leading to much higher working temperatures [33]. Furthermore, in most cases, concentrating collectors include a sun-tracking system, which adjusts the tilt angle according to the sun's position, aiming at a perpendicular incidence of the solar beams to the collector maximizing the absorbed solar irradiance [34]. From the available collector types, PTC and PDC are selected and modeled as the most common options that respond effectively in the examined temperature interval (150–250 °C).

The solar collectors' efficiency (η_{col}) can be computed by using empirical polynomial expressions that correlate it with the solar irradiance (I_b) and temperature difference between the fluid in the collectors' circuit (T_{col}) and the ambient temperature (T_{amb}) [35]:

$$\eta_{col} = c_0 - c_1 \frac{T_{col} - T_{amb}}{I_{sol}} \tag{1}$$

The values of coefficients c_0, c_1 that are used in the present study are listed in Table 2.

Table 2. Collectors' efficiency coefficients for each type of collector.

Coefficient	PTC [36]	PDC [37]
c_0 (-)	0.673	0.7053
c_1 (-)	0.2243	1.2503

Based on the definition of the collectors' efficiency, the heat absorbed by the collectors can be determined through the following equation:

$$\eta_{col} = \frac{\dot{Q}_{col}}{A_{col} I_{sol}} \Rightarrow \dot{Q}_{col} = \eta_{col} A_{col} I_{sol} \tag{2}$$

Eventually, the enthalpy (and thus the temperature) at the outlet of the collectors can be determined by applying the energy balance equation:

$$h_{col,o} = h_{col,i} + \frac{\dot{Q}_{col}}{\dot{m}_{col}} \tag{3}$$

For both types of solar collectors, it was decided to consider a sun tracking system to maximize the absorbed solar energy. A single-axis tracking mechanism was considered, in which the collectors are fixed with respect to the North-South axis and rotate around an axis in the direction East-West.

2.2. Thermal Energy Storage Tank

The developed model for the thermal energy storage (TES) system is based on the assumption of the thermal stratification of the tank [38]. The tank is considered to be

separated into horizontal zones inside each of which the HTF has a uniform temperature, as shown in Figure 2a. Between the zones, heat and mass transfer phenomena take place, which contribute to its temperature gradient, according to mass and energy balance in each zone [39].
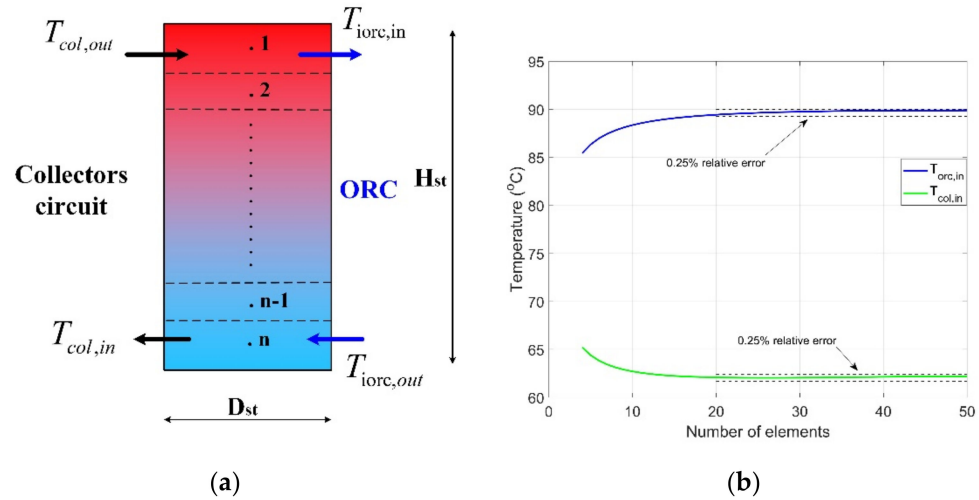

Figure 2. (**a**) Schematic of the storage tank's discretization methodology; (**b**) overview of the influence of the number of mixing zones on the stability of the solution.

Concerning the modeling of the storage tank, the assumption of a number ($n = 25$) of mixing zones was considered as shown in Figure 2b so that a maximum relative error of 0.25% is attained in the calculation of the HTF supply temperature to the ORC evaporator and the solar collectors [40]. The selection of this number of elements was dictated by the fact that both exiting streams had a deviation of less than 0.2 K from the estimated value when the double ($n = 50$) elements were used. Moreover, a relatively small number of elements reduces the computational costs, as this function has to be solved 8760 times for every case study. Assuming a uniform temperature within each mixing zone, an energy balance is applied at the boundaries of each zone [39,41]. For a total of 25 zones at each time step t, the energy balance equations at each timestep t are:

For the upper zone, j = 1:

$$\frac{M_{st}}{25}\frac{h_{st,(t,1)}-h_{st,(t-1,1)}}{\Delta t} = \dot{m}_{col}\left(h_{col,o}-h_{st,(t,1)}\right) + \dot{m}_{iorc}\left(h_{st,(t,2)}-h_{st,(t,1)}\right) - U_l A_{st,1}\left(T_{st,(t,1)}-T_{amb}\right) \tag{4}$$

For the intermediate zones, j = (2, 3, . . . , 24):

$$\frac{M_{st}}{25}\frac{h_{st,(t,j)}-h_{st,(t-1,j)}}{\Delta t} = \dot{m}_{col}\left(h_{st,(t,j-1)}-h_{st,(t,j)}\right) + \dot{m}_{iorc}\left(h_{st,(t,j+1)}-h_{st,(t,1)}\right) - U_l A_{st,j}\left(T_{st,(t,j)}-T_{amb}\right) \tag{5}$$

For the bottom zone, j = 25:

$$\frac{M_{st}}{25}\frac{h_{st,(t,25)}-h_{st,(t-1,25)}}{\Delta t} = \dot{m}_{col}\left(h_{st,(t,24)}-h_{st,(t,25)}\right) + \dot{m}_{iorc}\left(h_{iorc,o}-h_{st,(t,25)}\right) - U_l A_{st,25}\left(T_{st,(t,25)}-T_{amb}\right) \tag{6}$$

The heat loss coefficient of the storage tank to its surroundings, U_l, was assumed to be equal to 2.5 W m^{-2} K^{-1} [42].

For both sub-circuits interconnected with the storage tank, the same HTF was selected based on the maximum working temperatures. The selected HTF is Therminol VP-1, which is commonly used at temperatures above 250 °C since its maximum working temperature is approximately 327 °C [43,44]. The operating strategy of the solar subsystem is depicted in Figure A1 of Appendix A.

2.3. Organic Rankine Cycle

2.3.1. Component Simulation Models

Heat Exchangers

The layout of the ORC includes three heat exchangers; the evaporator, condenser and recuperator. Their on-design modeling is based on the selection of the appropriate commercial plate heat exchanger that satisfies the needs in terms of the heat transfer surface and has an acceptable pressure drop on both streams.

The sizing of heat exchangers is based on the LMTD method [45]. The Nusselt number for the heat transfer during evaporation is estimated using the correlation of Yan and Lin [46]:

$$Nu = 19.26 Re_L^{0.5} Bo_{eq}^{0.3} Pr_L^{1/3} \tag{7}$$

Regarding the calculation of the pressure drop on each channel, the equation of Focke [47] is applied:

$$\Delta p_{ch} = \frac{f L_p}{D_h} \frac{\rho_{ch} v_{ch}^2}{2} \tag{8}$$

The friction factor for the evaporator is derived from different expressions according to the range within which the Reynolds number lies [46,48]

$$f = \begin{cases} 6.1 \cdot 10^4 \cdot Re_{eq}(n)^{-1.25}, Re_L(n) < 750 \\ 6.947 \cdot 10^5 \cdot Re_L(n)^{-0.5} Re_{eq}(n)^{-1.109}, Re_L(n) \geq 750 \text{ and } Re_{eq}(n) < 6000 \\ 31.21 Re_L^{-0.5} Re_{eq}^{0.04557}, otherwise \end{cases} \tag{9}$$

For the condenser, the correlations used to calculate the Nusselt number and the friction factor are those of Thonon [49] and Han [50], respectively:

$$Nu = 0.5331 \frac{\lambda}{D_h} Re_{eq}^{-0.76} Pr_L^{1/3} Re_L^{0.653} \tag{10}$$

$$f = 3521.1 \left(\frac{\Lambda}{D_h}\right)^{4.17} \left(\frac{\pi}{2} - \varphi\right)^{-7.75} Re_L^{Ge_4} \tag{11}$$

$$Ge_4 = -1.024 \left(\frac{\Lambda}{D_h}\right)^{0.0925} \left(\frac{\pi}{2} - \varphi\right)^{-1.3} \tag{12}$$

Finally, for the case of the recuperator, as well as of a single-phase heat transfer process, the Nusselt number derives from the correlation of Donowski and Kandlikar [51], whereas Thonon's friction factor is used [52]:

$$Nu = 0.2875 Pr_L^{1/3} Re^{0.78} \tag{13}$$

$$f = \begin{cases} 45.57 Re^{-0.67}, Re < 160 \\ 0.37 Re^{-0.172}, Re > 160 \end{cases} \tag{14}$$

Pump

A positive displacement diaphragm pump is considered, whose basic technical characteristics are presented in Table 3, as they are derived from its technical datasheet [53].

Table 3. Design specifications of Hydra Cell G25-E pump [53].

Property	Value
Maximum flow rate (lt/min)	75.9
Maximum discharge pressure (bar)	69
Maximum inlet pressure (bar)	17
Maximum operating temperature (°C)	121

Based on the data provided by the manufacturer, the rotational speed, the mechanical power loads and the total electrical consumption of the pump can be estimated by Equations (14)–(16):

$$N_{pump} = 14.6574 \dot{V}_{pump} + 1.2586 \tag{15}$$

$$\dot{W}_{mech,pump} = \frac{50 N_{pump}}{84428} \frac{\dot{V}_{pump} \Delta p}{511} \tag{16}$$

$$\dot{W}_{el,pump} = \frac{\dot{W}_{mech,pump}}{\eta_{el,motor} \eta_{el,inv}} \tag{17}$$

In the above Equations (15) and (16), the rotational speed, the volumetric flowrate and the pressure difference are expressed in rpm, bar and lt/min, respectively.

The expander's generator and the pump's motor are both considered to be connected with an inverter. The correlations derived from the study by Ziviani et al. [54] are used for the estimation of their efficiencies. More details on these equations are listed in a previous study conducted by the authors [55].

Expanders

The investigated ORC is intended for operation at medium to high-temperature range, and thus a conventional hermetic screw expander was considered. A correlation between the isentropic efficiency and the pressure ratio of the screw machine was derived based on the experimental data of the study by Hsu et al. [56], in which the performance of a screw expander coupled with an ORC system for various working conditions was investigated. Due to the limitations of the pressure ratio of screw machines, it was considered that the system may contain a maximum of two expanders functioning with a pressure ratio varying between 2.4 and 6.1 [56,57]. The correlation between the isentropic efficiency of a screw expander and its pressure ratio (r_p) is the following:

$$\eta_{is,exp} = 0.001082 r_p^5 - 0.027767 r_p^4 + 0.2871 r_p^3 - 1.51052 r_p^2 + 406965 r_p - 3.78 \tag{18}$$

Thus, when the high and low pressures of the ORC are known, the isentropic efficiency of the expander can be calculated from Equation (18), considering that both expanders work at the same pressure ratios, equal to the square root of the ORC's high pressure to low pressure ratio. In order to estimate the power production in the expanders, the losses involved in the expansion process have to be considered. Apart from the isentropic efficiency, the inverter's and the generator's efficiencies, there has to be a term for the heat losses in the expander. In literature, there is a large deviation in the estimated heat losses of the expanders. For example, Wang et al. [58] reported heat losses of up to 0.65 kW for a screw expander of approximately 7 kWe (9.2%). Lemort et al. [59] measured the heat losses for a scroll expander at almost 4%, while the study from Giuffrida [60] estimated losses to the ambient of more than 6%. Due to these deviations, this study considered an average value for the heat losses, in the range of 5%. Hence, the net produced power in the expander can be calculated by the following expression:

$$\dot{W}_{el,exp} = 0.95 \eta_{is,exp} \dot{W}_{is,exp} \eta_{el,gen} \eta_{el,inv} \tag{19}$$

The displacement volume of the expander, required for the cost estimation of the expander, is calculated, taking into consideration the definition of its filling factor:

$$V_s = \frac{60 \dot{m}}{N_{exp} \rho_{exp,i} ff} \tag{20}$$

The value of the filling factor is derived by applying a polynomial expression based on the experimental data presented by Dumont et al. [61], as shown in Figure 3.
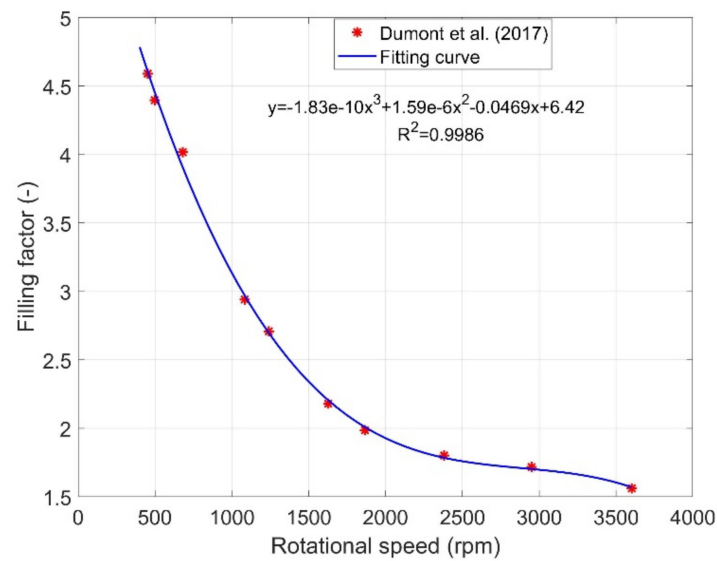
Figure 3. Filling factor as a function of the rotational speed based on data from Dumont et al. [61].

2.3.2. ORC Design

General Assumptions

The aforementioned models are used to calculate the on-design thermodynamic states at each point of the cycle and size the equipment components, according to the assumptions and boundary conditions summarized in Table 4 and the layout of the cycle shown in Figure 1. An optimization algorithm is implemented to estimate the optimal subcritical cycle conditions in order to maximize the thermal efficiency of the cycle, which is defined according to the following equation:

$$\eta_{th} = \frac{\dot{W}_{el,exp} - \dot{W}_{el,pump}}{\dot{Q}_{evap} - \dot{Q}_{rec}} = \frac{\dot{W}_{el,net}}{\dot{Q}_{evap} - \dot{Q}_{rec}} \quad (21)$$

Table 4. On-design working parameters of ORC.

Property	Value
Evaporator heat duty (kW)	40.0
Heat exchangers pinch point (K)	5.0 ÷ 40
Condenser subcooling (K)	5.0
HTF inlet temperature (°C)	210
HTF inlet pressure (bar)	1.5
HTF mass flow rate (kg/s)	0.8
Single expander pressure ratio (-)	2.4 ÷ 6.1
Cooling water inlet temperature (°C)	20.0
Cooling water inlet pressure (bar)	2.0
Cooling water mass flow rate (kg/s)	1.0

In the above formula, the difference in the denominator is the final heat supplied to the evaporator, which is equal to the initially imposed evaporator's heat duty reduced by the heat duty of the recuperator.

The independent design variables of the ORC are the evaporation and condensation pressure as well as the mass flowrate of the working fluid. These variables were selected by taking into account the boundary conditions and constraints that are presented in Table 4.

A dedicated single objective optimization algorithm is executed to find the optimal specifications of the ORC cycle for each of the considered working fluids towards the maximization of the cycle's thermal efficiency, presented in Section 4.1. The on-design algorithm, shown in Figure A2 of Appendix A, is based on the assumption of a mass flow rate and the evaluation of different levels of superheating, which define the high

pressure of the ORC cycle for the set driving temperature (HTF inlet), and different values of pressure ratios, which eventually lead to the estimation of the low pressure as well. As initial values, 15 K of superheating and a pressure ratio of 6 were set. The individual ORC component models are then solved sequentially, starting from the evaporator and ending in the pump. The feasibility of the solution is then evaluated based on the resulting pinch points of the heat exchangers. Once a solution delivers feasible pinch points (>5 K) in all heat exchangers, the mass flow is calculated by the solver to minimize the energy balance residual. Finally, a resizing of the evaporator and the condenser takes place to realize the requested heat transfer processes with the final mass flow of the ORC working fluid.

Depending on the operating conditions, a second expander is considered when the pressure ratio of the cycle is higher than the maximum expansion ratio of a single expander (set at 6.1). Meanwhile, a recuperator is operational when the temperature difference between the expander outlet temperature and the condensation temperature is greater than 20 K. Both the second expander and the recuperator can be bypassed if their operating criteria are not met with the addition of two diverting three-way valves.

Working Fluid Selection

The working fluid selection is based on critical properties and thermodynamic efficiency. In the present study, the thermodynamic efficiency at the nominal operating point was the main selection criterion. In most applications, the maximum efficiency is attained with fluids whose critical temperature is slightly higher than the cycle's driving temperature, to achieve maximum heat source utilization [62]. The considered working fluids are natural hydrocarbons, which have low cost and are very environmentally friendly owing to their extremely low global warming and zero ozone depletion potential. Although the particular working fluids are flammable, they could be employed in ORC systems if adequate safety measures are taken, as they are commonly used in commercial ORC plants. As shown in Figure 4, working fluids are distinguished into wet (i.e., working fluids which have a negative saturated vapor line in the temperature-entropy diagram) and dry (i.e., working fluids which have a positive saturated vapor line in the temperature-entropy diagram). In the present work, all considered fluids are dry to avoid droplet formation during expansion.
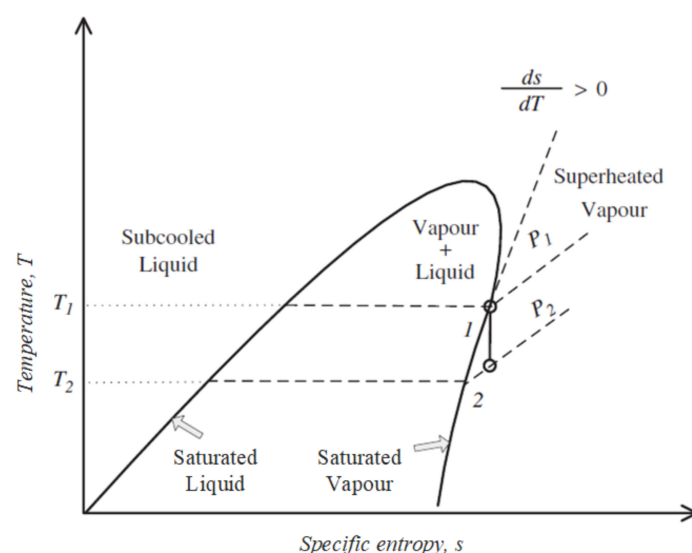

Figure 4. Temperature vs. specific entropy saturation curve of a dry fluid [63].

Furthermore, the use of the recuperator is more beneficial in the case of these fluids [64]. Since the maximum temperature of the solar loop is around 210 °C, only fluids with critical temperatures higher than this value were examined in the study. Although fluids with critical temperatures above 300 °C cannot be effectively coupled with the HTF, some

notable fluids with wide commercial application and critical temperatures exceeding this value were also assessed [40] for the sake of completeness. The list of the considered working fluids along with their critical properties and their type are presented in Table 5. The fluids that are selected for the main analysis of the study are highlighted in grey. These include the fluids yielding the highest efficiency values, as well as Toluene, which has extensive use in commercial ORC systems [44]. Since, according to Equation (18), expander efficiency is almost constant, exceeding 70%, for pressure ratios higher than 4, and since the examined cycles correspond to two-stage cycles with the pressure ratios of both machines above 4, the difference is derived from the isentropic enthalpy difference during expansion and the pump's consumption. The former is a property of the fluid and is maximized for the selected fluids whereas the latter depends on the volume flow rate and the difference between evaporation and condensation pressures. Although the pressure difference is higher for the selected fluids, they exhibit a higher expansion enthalpic difference, which outperforms the increased pump consumption.

Table 5. Properties and calculated design thermal efficiency of the examined organic fluids [65,66].

Organic Fluid	T_{crit} (°C)	p_{crit} (bar)	Fluid Type	p_{evap} (bar)	$T_{max,orc}$ (°C)	p_{cond} (bar)	$\dot{W}_{el,net}$ (kW)	η_{th} (%)
Isohexane	225	30.4	Dry	20.47	203.2	0.55	5.16	17.01
Acetone	235	47	Dry	25.24	199.5	0.68	6.07	15.17
Hexane	235	30.34	Dry	17.18	201.9	0.46	5.14	16.78
Cyclopentane	239	45.71	Dry	24.99	200.7	0.67	6.17	17.24
Methanol	240	82.16	Wet	12.04	204.7	0.32	5.74	14.14
Ethanol	242	62.68	Wet	23.02	204.9	0.62	5.34	12.9
Heptane	267	27.3	Dry	9.10	202.7	0.24	4.70	16.02
Cyclohexane	280	40.82	Dry	12.24	199.2	0.33	5.52	17.02
Benzene	289	48.9	Dry	12.82	198.0	0.34	5.90	16.39
MDM	291	14.1	Dry	2.80	201.3	0.08	3.34	13.77
Octane	296	25	Dry	4.93	199.8	0.13	4.35	15.1
Toluene	319	41.3	Dry	6.53	197.4	0.18	5.37	15.71
n-Nonane	321	22.7	Dry	2.80	193.9	0.08	4.05	14.21
p-Xylene	343	35.3	Dry	3.66	196.7	0.09	4.92	14.88

In order to account for the fluctuations in the driving temperature, the off-design operation of the system is simulated. The lowest HTF temperature which is the threshold for the operation of the ORC system is taken equal to 180 °C (T_{thr}). Thus, as the HTF varies from 180 °C to 210 °C the heat absorbed by the evaporator varies from 20 kW_{th} to its nominal value of 40 kW_{th}. For intermediate HTF temperatures between 180 and 210 °C, a linear variation of the heat input to the ORC is considered. A detailed analysis of the off-design modeling of the system accompanied by a flowchart is included in Appendix A.

2.4. Cost Estimation

Several cost correlations are used for calculating the cost of system components. Because these correlations have different reference years, they are modified by taking into account the inflation rate to convert their outputs from their respective reference years to 2019-equivalent monetary values.

The specific purchase cost (€/m²) of PTCs and PDCs is displayed in Table 6.

Table 6. Solar panels' specific costs based on data from literature.

Type of Collector	PTC [67]	PDC [68,69]
Specific price (€/m²)	178 (in €2015)	235 (in €2010)

The cost correlations shown in Table 7 are used for calculating the cost of the ORC equipment components.

Table 7. Cost correlations for system's components (all correlations are adapted to €2019 equivalent values).

Component (Year of Value)	Correlation	
Pipelines (€2013) [70]	$C_{pip} = \left(0.89 + 0.21 D_{pip}\right) L_{pip}$	(22)
Storage tank (€2020)	$C_{st} = 1129 V_{st} + 82.8$	(23)
ORC hardware/Miscellaneous (€2020) * [62]	$C_{misc,ORC} = 800$	(24)
Receiver (€2016) [71]	$C_{rt} = 4.48 V_{rt} + 150.46$	(25)
Pump (€2013) [70]	$C_{pump} = 900 \left(\dfrac{\dot{W}_{mech,pump,nom}}{300,000} \right)^{0.25}$	(26)
Motor/Generator (€2015) [72]	$C_{gen} = 71.7 \left(\dfrac{\dot{W}_{el,exp}}{1000} \right)^{0.95}$	(27)
Expander (€2014) [73]	$C_{exp} = 0.88(3143.7 + 217423 V_s)$	(28)
Heat exchangers (€2011) [62]	$C_{hex} = 190 + 310 \left(A_{evap} + A_{cond} + A_{rec} \right)$	(29)
Installation (€2020) [62]	$C_{ins} = 0.2 \cdot CAPEX$	(30)

* As the hardware of the ORC is conventional equipment, no inflation was considered in this case.

The cost of the working fluids and HTF Therminol VP-1 is calculated according to market price data (Table 8).

Table 8. Specific cost of working fluids and heat transfer fluid Therminol VP-1 (in €2020).

Working Fluid	Cyclopentane [74]	Cyclohexane [75]	Isohexane [76]	Hexane [77]
Specific price (€/lt)	1.32	2.84	0.85	0.82

Working Fluid	Benzene [78]	Toluene [79]	Therminol VP-1 (HTF) [80]	
Specific price (€/lt)	1.09	0.92	4.78	

The HTF volume in the solar circuit is calculated based on the solar field surface and storage tank capacity (as the storage tank is considered to be filled with HTF), according to the following equation:

$$V_{HTF} = V_{st} + 0.12 A_{col} + 0.05 \qquad (31)$$

The factor 0.12 is a typical value provided by a manufacturer, while the added constant of 0.05 is an approximation for the intermediate pipelines between the solar field, the storage tank and the ORC evaporator. The quantity of working fluid used in the ORC is calculated based on its capacity and the size of heat exchangers, as well as the requirement of an 80 lt receiver tank, in accordance with experience from similar experimental systems [81–83]. Overall, the total amount of working fluid is taken equal to 1.5 times the total capacity of the receiver tank (120 lt).

2.5. Performance Indicators-Optimization Objectives

Two performance indicators are used, which are also the optimization objectives. The first is the total solar conversion efficiency (η_{tot}), which accounts for the total solar energy harvested over a complete year of operation:

$$\eta_{tot} = \frac{\int \left(\dot{W}_{el,exp} - \dot{W}_{el,pump} \right)}{\int \dot{Q}_{sol}} = \frac{\int \dot{W}_{el,net}}{\int \dot{Q}_{sol}} \qquad (32)$$

$$\dot{Q}_{sol} = I_{sol} A_{col} \qquad (33)$$

The thermodynamic assessment of the designed system is coupled with the corresponding economic evaluation to estimate its economic viability. In order to allow for a direct comparison of the proposed system with alternative energy production technologies, the economic performance is evaluated with respect to its Levelized Cost of Electricity (LCoE). LCoE is one of the most commonly used economic evaluation indexes and can be

used for the comparison of energy production systems of various technologies [84]. It is computed by dividing the electricity generation costs, reduced in an annual period, by the annually produced electrical energy and reflects the cost of the produced energy within the system's lifetime:

$$LCoE = \frac{\frac{CAPEX \cdot i}{1-(1+i)^{-n}} + OPEX}{\dot{W}_{el,net}} \tag{34}$$

In the above equation, CAPEX is the total capital expenditure of the system, while OPEX represents the annual operational expenses, which are taken equal to 2% of the CAPEX. Meanwhile, a discount rate (*i*) equal to 5% is assumed, while the system lifetime (*n*) is considered equal to 25 years.

In each case, the calculated LCoE values are compared to the national electricity prices for private household consumers of the selected cities [85], as shown in Table 9. It should be noted that these electricity prices are determined by the electricity mix (which is dominated by mature, cost-effective power generation technologies with minimal marginal costs) and by the electrical energy imports/exports of the countries as well as policy factors. It is thus expected that these prices will be substantially lower than the cost of the investigated solar ORC, which is a non-commercialized technology with a low technology readiness level (TRL). Therefore, the electricity prices are used in the present study only to provide a preliminary comparison basis of the LCoE of the solar ORC and should not be interpreted as strict economic evaluation indicators. However, it has to be noted that as EU directive 2018/2021 [86] promotes the increased penetration of renewables and the consequent reduction in low-cost fossil-derived energy, the electricity prices are expected to increase in the near future, towards the benefit of the proposed solar ORC solution.

Table 9. Electricity prices for private household consumers in the selected countries for 2020 (€/kWh) based on data from Eurostat [85].

Country	Greece	Spain	Italy	Belgium	Germany
Electricity price, c_{el} (€/kWh)	0.1641	0.2298	0.2153	0.2702	0.3006

2.6. Genetic Algorithm Optimization

A multi-objective genetic algorithm was implemented to optimize the system's performance with two objective functions: (a) the system's total efficiency (η_{tot}) which must be maximized, and (b) the Levelized Cost of Energy (LCoE) which must be minimized. Two independent optimization variables are considered: the collectors' surface (A_{col}) and the storage tank's capacity (V_{st}). The boundaries for the genetic algorithm's variables are listed in Table 10. The initial solar field area and tank capacity are 120 m^2 and 3.0 m^3, respectively, as the ratio of 40 m^2/m^3 is commonly applied in solar-driven applications with TES [87]. The population of each generation was equal to 50, which is a sufficient number of offspring for a two-variable problem. The optimization was set to terminate after 20 generations.

Table 10. Genetic algorithm optimization variable boundaries and initial values.

Parameter	Range
Solar collectors' field (m^2)	10 ÷ 400
Initial solar collectors' surface (m^2)	120
Storage tank capacity (m^3)	0.2 ÷ 5.0
Initial storage tank capacity (m^3)	3.0

Overall, 60 scenarios were evaluated, consisting of the five cities, six working fluids/ORC nominal designs and two types of collectors.

3. Results

All results are available in the Supplementary Materials of the present publication. The Pareto fronts of the solutions produced by the GA are shown in Figure 5. The shape of the fronts illustrates that there is a trade-off between the optimization criteria of efficiency and LCoE [88]. Indeed, the energy efficiency maximization and the LCoE minimization are independent and in certain cases conflicting objectives. For example, a small-sized system may achieve high annual solar conversion efficiencies, but the produced electricity may not necessarily be sufficient to compensate for its investment cost, negatively affecting its cost-effectiveness. Regarding the investigated solar ORC, increasing the area of solar collectors enables the ORC to operate closer to its nominal point (and hence at higher thermal efficiency) for longer periods, leading to an increase of the total solar thermal conversion efficiency. However, the increased generated electricity does not necessarily compensate for the higher cost of the solar field. Accordingly, increasing the storage tank volume extends the capacity factor of the system and results in increased solar thermal conversion efficiencies, but the increased cost of the tank may lead to disproportionately increased capital costs and have a negative influence on the LCoE.
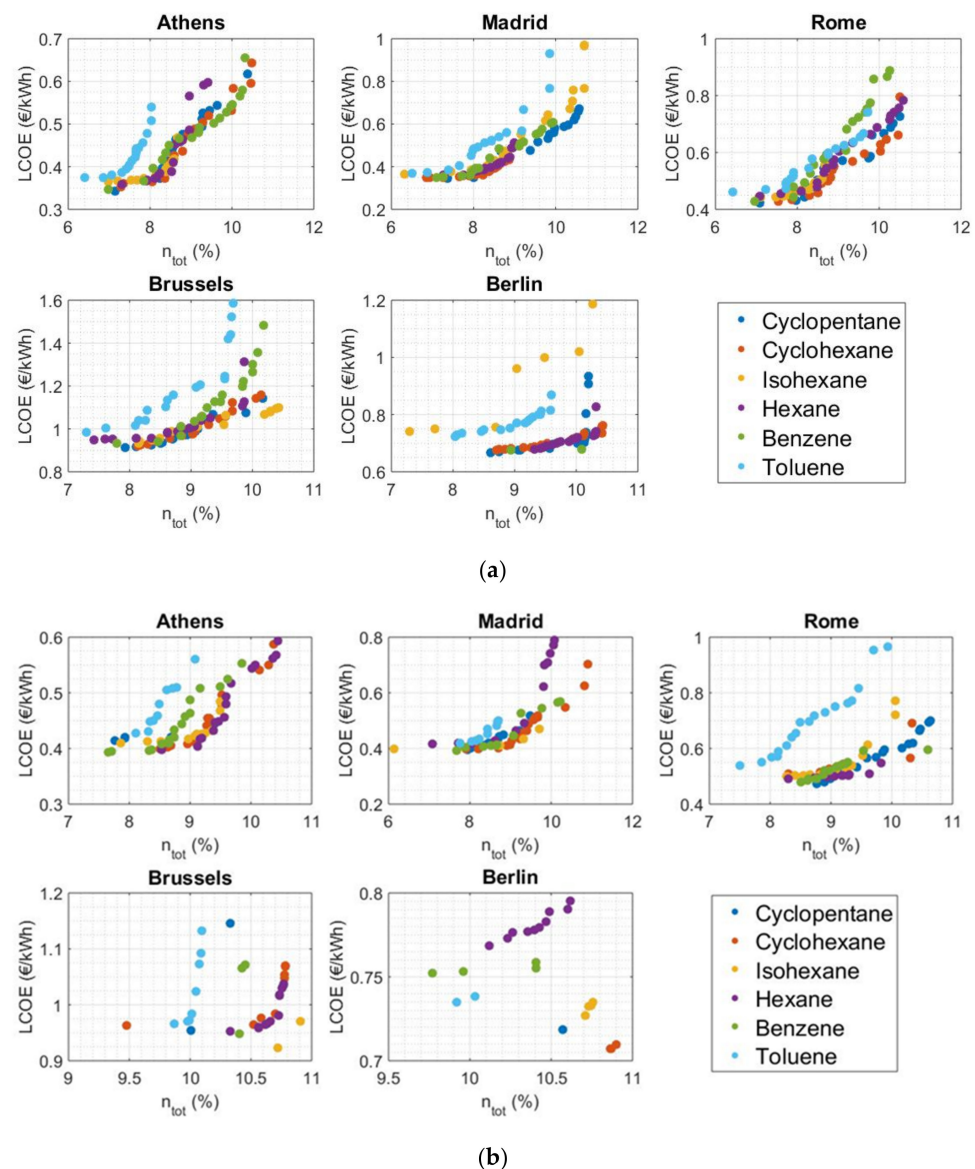
Figure 5. Pareto fronts (LCoE-η_{tot}) for the considered working fluids in the examined cities for (**a**) PTCs and (**b**) PDCs.

The above point is illustrated more clearly in Figure 6, which presents the optimization results for an indicative scenario of Athens with PTCs for all the examined working fluids. In this figure, the variation of the two optimization objectives (η_{tot} and LCoE) with respect to the two optimization variables of the system (A_{col} and V_{st}) is illustrated.
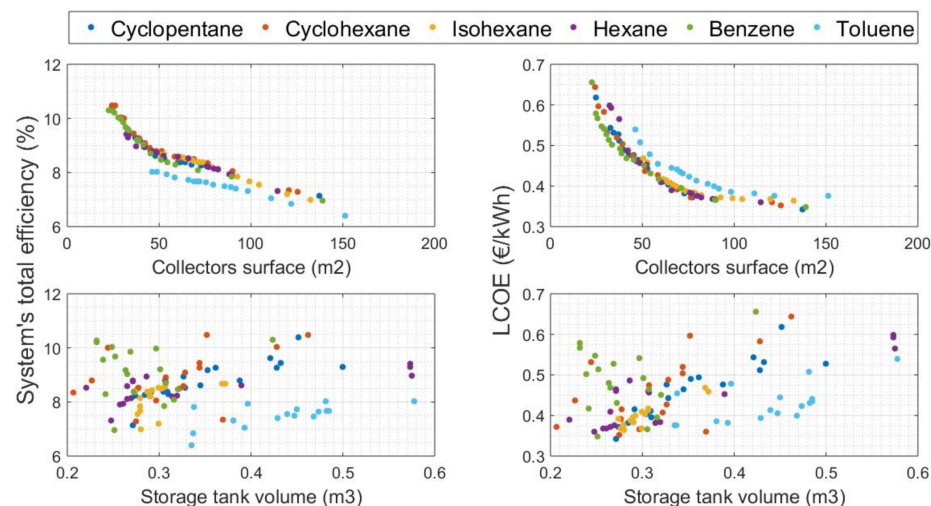

Figure 6. Variation of the optimization objectives (LCoE and η_{tot}) as a function of the optimization variables (A_{col} and V_{st}) for a PTC-driven system in Athens for the investigated working fluids.

3.1. Total Energy Efficiency

It can be observed that higher total conversion efficiencies are obtained in northern cities (Brussels and Berlin) compared to southern cities (mainly Athens and Madrid). Since in all cases the nominal size of the ORC is the same, due to the lower solar availability in Northern cities, the ORC directly exploits the harvested solar energy. On the contrary, in Southern cities, a large share of the harvested solar heat is stored and eventually lost to the ambient. Furthermore, the lower ambient temperatures in Northern cities lead to lower solar collector losses.

It can be observed that the use of different working fluids does not lead to substantial differences in efficiencies. Generally, Cyclohexane tends to achieve the highest performance, followed by Cyclopentane and Isohexane. In most cases, Toluene appears to yield slightly inferior efficiencies followed by Benzene. The overall maximum efficiency achieved in the studied cities lies between 10.5–11%. These values are, in general, lower than those reported in similar studies. This can be mainly attributed to the fact that the present work takes into detailed account different types of losses, including the heat losses to the ambient, pump, inverters' and generators' losses, which are often underestimated or even neglected.

Finally, it can be observed that, although PDCs lead to slightly higher efficiencies compared to PTCs, the difference in the performance of systems operating with these two types of collectors is insignificant.

3.2. LCoE

The influence of the geographical location on the LCoE is much more significant than its influence on the total conversion efficiency. As already mentioned, for southern cities, the available solar energy is higher, leading to higher power generation and enabling system operation for more hours annually and closer to nominal conditions. The increased electricity generation results in increased cash inflows and reduced LCoE values, improving the economic viability of the system. More specifically, in the case of Athens and Madrid, which represent the financially optimal results, the cost of electricity for the PTC-Cyclopentane scenario is close to 0.34 €/kWh, whereas the corresponding LCoE in Brussels is 0.9 €/kWh.

In the majority of the scenarios, the optimal financial outcome is achieved by the fluids that yield the highest efficiencies, as Cyclopentane and Cyclohexane exhibit the highest profitability, whereas Toluene, Benzene and Hexane are associated with lower cost-effectiveness. Since the fluids are hydrocarbons and have similar prices, their costs do not lead to substantial differentiation in their economic competitiveness, which is mainly ruled by their thermodynamic performance and equipment sizing and, hence, costs.

From an economic perspective, PTCs are more favorable, since they have almost the same energetic performance but come at a lower cost than PDCs.

4. Discussion

4.1. Interpretation of Optimization Results

An overview of the results is presented in Table 11, in which the combinations of optimal solar field areas and storage tank capacities with regard to efficiency and LCoE for each city are shown.

Table 11. Optimal working fluids, collector types, solar field areas and storage tank volumes that maximize total solar conversion efficiency and minimize levelized cost of electricity in each of the examined cities.

City	Objective	Working Fluid	Collector Type	η_{tot} (%)	LCoE (€/kWh)	A_{col} (m^2)	V_{st} (m^3)	c_{el} (€/kWh)
Athens	max η_{tot}	Cyclohexane	PTC	10.49	0.6432	24.37	0.46	0.1646
Athens	min LCoE	Cyclopentane	PTC	7.14	0.3432	137.32	0.27	0.1646
Madrid	max η_{tot}	Cyclohexane	PDC	10.9	0.7034	20.81	0.33	0.2477
Madrid	min LCoE	Cyclopentane	PTC	7.37	0.3444	120.84	0.33	0.2477
Rome	max η_{tot}	Cyclopentane	PDC	10.64	0.7010	29.9	0.37	0.2161
Rome	min LCoE	Cyclopentane	PTC	7.08	0.4214	150.84	0.30	0.2161
Brussels	max η_{tot}	Isohexane	PDC	10.91	0.9706	84.22	0.22	0.2937
Brussels	min LCoE	Cyclopentane	PTC	7.93	0.9146	146.1	0.31	0.2937
Berlin	max η_{tot}	Cyclohexane	PDC	10.9	0.7096	149.92	0.23	0.3000
Berlin	min LCoE	Cyclopentane	PTC	8.61	0.6661	211.69	0.26	0.3000

As it can be observed in Figure 6, the collecting surface appears to be negatively correlated with both η_{tot} and LCoE. When the surface is too small, the useful solar heat is reduced. As a result, the harvested solar energy is fully used directly for driving the ORC, while the stored heat and thus storage tank energy losses are minimized. On the other hand, as the surface is increased, although more solar energy is harvested, a part is left unexploited and eventually lost to the ambient from the storage tank due to the fixed nominal size of the ORC.

Accordingly, for smaller collector areas, the annually generated electrical energy is lower because the system is operational for fewer hours, resulting in a decreased cashflows and increased LCoE. On the contrary, for larger collector areas, the ORC operates for longer periods at higher efficiencies, producing more electrical energy and thus the LCoE is reduced.

As shown in the figures, the solar field area corresponding to the optimal economic performance is around 150 m^2. For larger areas, the improvement in the economic competitiveness of the system is negligible, since the CAPEX is increased while the electrical energy generation remains almost constant. This region is not depicted in the diagrams since it corresponds to both minimized efficiency and financial performance.

Concerning the volume of the storage tank, it is positively correlated with the energy efficiency, since higher volumes result in increased system operating hours and thus higher energy exploitation. However, given a specific collecting area, an increase in the storage capacity beyond a specific value does not offer any more benefits and even increases the CAPEX, resulting in a stall of economic and energy efficiency.

Additionally, it can be observed that the optimal results are concentrated in a range of relatively small storage tank capacities. This is justified both in terms of efficiency as well

as in terms of economic performance. It is obvious that the higher storage tank volumes increase the CAPEX, while at the same time they increase the thermal inertia of the system. Larger tanks would demand much higher thermal power from the collectors to increase their temperature since they contain larger quantities of HTF and have greater ambient losses. Therefore, even though the inspected range is between 0.2–5 m^3, in all cases the derived optimal points correspond to tank capacities below 1.2 m^3. Another reason for this behavior is justified by the selection of the heat losses coefficient of the tank. The value considered in this study corresponds to a medium-insulated tank, hence for high temperatures the heat losses are not negligible. If high insulation is considered, the total energy efficiency is expected to increase for the same tank size; however, this would lead to a significantly higher tank cost and may have either an either neutral or a negative impact on the LCoE.

Generally, the lowest LCoE values are attained in the southern cities, where the solar availability, and thus the total electrical energy generation, are higher.

Based on the results, it can be concluded that a major hindrance to the commercial uptake of the investigated solar ORCs is their limited financial viability. As shown in the table, the optimal LCoE for the examined cities ranges between 0.34–0.91 €/kWh. Meanwhile, as of 2019, the LCoE in the EU of PV technology, the main competitor to the investigated solar ORC concept, ranges from 0.0619 to 0.32 €/kWh [89], as illustrated in Figure 7, being considerably lower than the LCoE of the solar ORC.
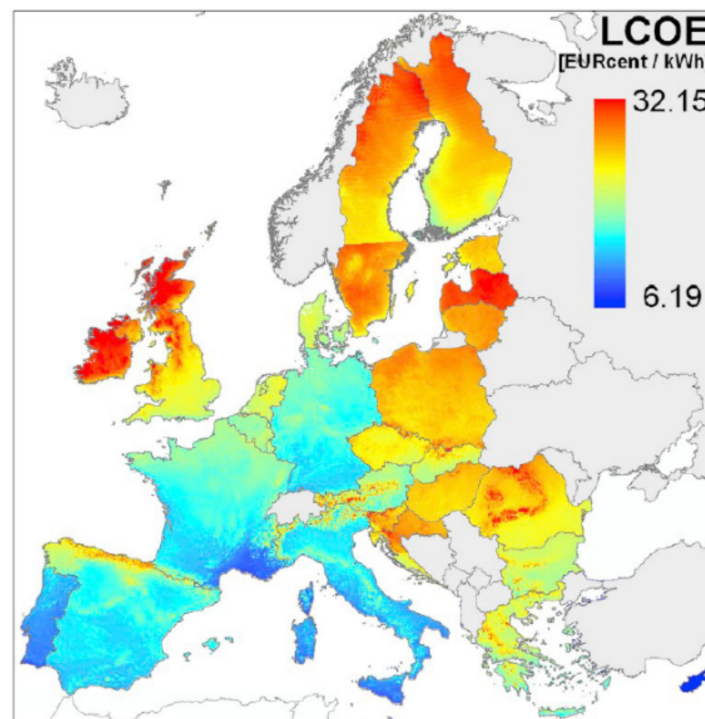

Figure 7. LCoE of PV-generated electricity in the EU as of 2019 [89].

Furthermore, the LCoE of the solar ORCs is much higher than the current electricity prices listed in Table 9. Of course, it should be noted that in the study, no policy incentives (such as subsidies or premiums) have been taken into account, which are very commonly introduced in RES systems and which could greatly improve the economic competitiveness of the investigated solar ORCs. Moreover, it is expected that the addition of heat production by recovering low-temperature heat from the condenser could enhance the cost-effectiveness at a small penalty of the ORC thermal efficiency. This is mainly because the condensation temperature is already relatively high due to the technical limitations of the expander's pressure ratios and therefore, under the current design, the cooling water outlet temperature is suitable for floor heating applications.

To provide a more detailed analysis of the system economics, the contribution of the cost of different components into the CAPEX is illustrated for the scenario that yields the economically optimal results of Athens for PTC and using Cyclopentane (as shown in Table 11) in the two pie charts of Figure 8. At this point, it has to be mentioned, according to Figure 8b and the specific costs of the HTF reported in Table 8, that the selection of Therminol VP-1 has a significant impact on the total costs, owing to the large quantity of the HTF used in the solar field. The use of this particular HTF is necessary due to the high solar field temperatures, which prohibit the use of less expensive HTFs such as ethylene or propylene glycol aqueous mixtures.
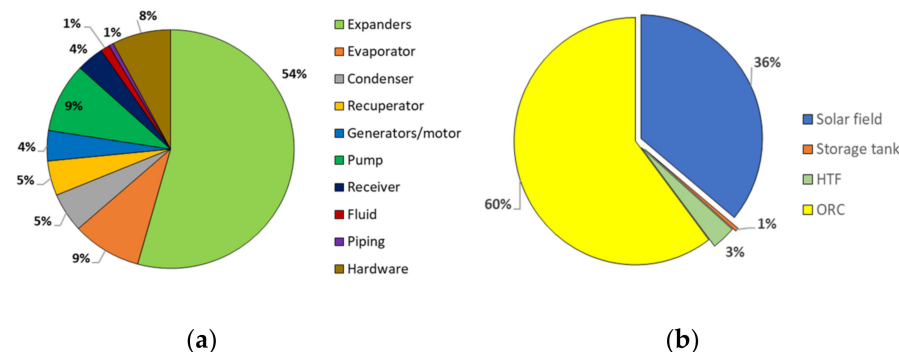

(**a**)   (**b**)

Figure 8. (**a**) Cost distribution of ORC components; (**b**) Cost distribution of sub-systems (results refer to the case of Athens–PTC–Cyclopentane for minimum LCoE (Table 11).

Among the ORC components, the biggest cost contribution is that of the screw expanders, followed by the evaporator and pump. When the total system cost is considered, more than half of its cost corresponds to the ORC module, with the solar field also having a strong contribution to the CAPEX.

4.2. Operational Improvements

In order to explore the economic viability of the designed system and determine its capability of achieving lower LCoE values, its economic performance under different nominal evaporator heat duties is presented. The analysis is only carried out for the case of a PTC-driven solar ORC in Athens operating with Cyclopentane, which corresponds to the minimum LCoE scenario. Four additional cases were examined regarding the nominal duty of the evaporator: 25 kW, 32.5 kW, 60 kW and 80 kW. In Figure 9 and Table 12, the optimal solar field area and storage tank volume for each nominal evaporator heat duty and corresponding LCoE and η_{tot} are presented.
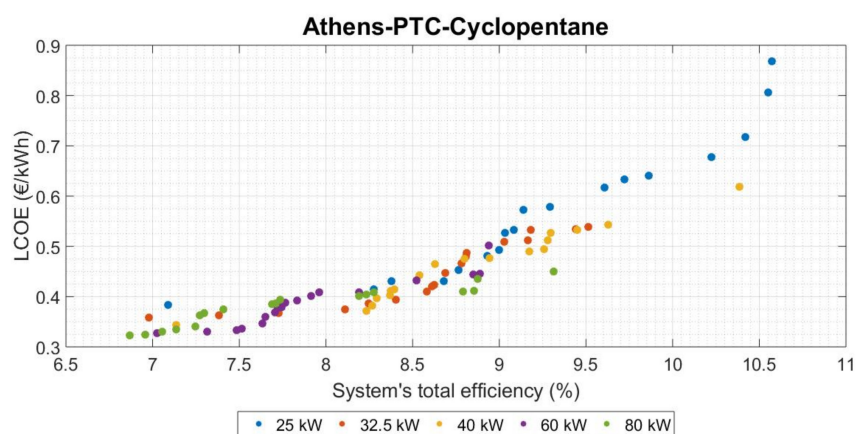

Figure 9. Pareto fronts of PTC-driven ORCs of different nominal heat input values located in Athens and operating with Cyclopentane.

Table 12. Variation of the minimum levelized cost of electricity, corresponding total solar conversion efficiency and optimal solar field area and storage tank volume for different nominal system heat input values (Athens, PTC, Cyclopentane).

$\dot{Q}_{evap}$ (kW)	min LCoE (€/kWh)	η_{tot} (%)	A_{col} (m²)	V_{st} (m³)
25.0	0.3839	7.09	100.16	0.32
32.5	0.3588	6.98	126.23	0.29
40.0	0.3432	7.14	137.32	0.27
60.0	0.3276	7.03	181.12	0.23
80.0	0.3229	6.87	219.64	0.28

For a given driving temperature, as the evaporator's heat duty decreases, the ORC power output is decreased. However, the lower accumulation of stored heat (for a given solar field area and storage tank volume) allows for a higher level of charging and therefore the ORC is operational for longer operating hours, thus achieving higher total solar energy conversion efficiencies. On the other hand, because of the decreasing size of the system, the specific investment cost of the equipment components is increased. Ultimately, the negative effect of the increasing specific investment cost is more significant than that of the increased operating hours, as indicated by the increasing LCoE for decreasing nominal evaporator heat duties.

As expected, there is a positive correlation between the optimal solar field area and the ORC nominal power output; as the ORC power scale increases more heat is required, respectively. However, a reverse behavior is observed for the storage tank volume. This can be attributed to the substantial costs of a larger storage tank and the respective additional HTF costs, which push the optimization algorithm toward lower storage tank capacities. In fact, in all cases shown in Table 12 and Figure 10, the optimal economic performance occurs at low tank capacities. As the profit by sold electricity was not considered to vary within the day, it is more economically efficient to directly consume the solar harvested energy. In this perspective, the storage tank is mostly used to provide the required thermal inertia in the system to allow it to operate at steadier and closer to nominal conditions and therefore 200–300 lt are sufficient.
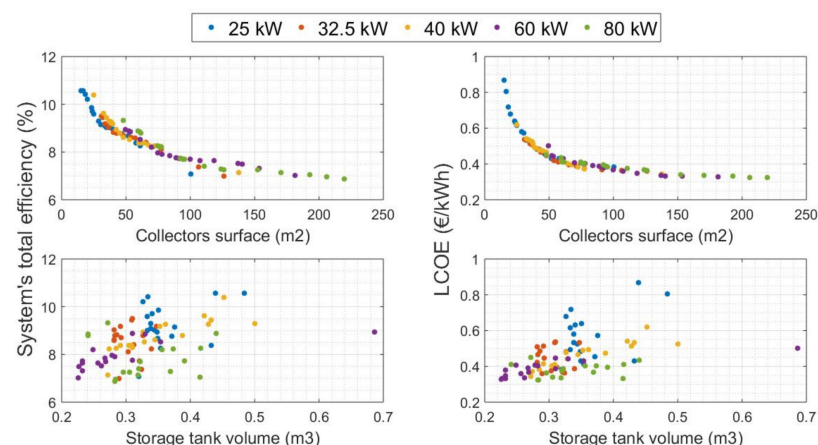

Figure 10. Variation of the optimized total solar conversion efficiency and levelized cost of electricity as a function of the solar collectors' surface and storage tank volume for PTC-driven ORCs of different nominal heat input values located in Athens and operating with Cyclopentane.

By observing the trends of Figure 10, it can be deduced that a further increase in the system scale accompanied by an increase in the collecting surface could eventually lead to even lower LCoE values. However, further increasing the evaporator heat duty beyond this value would require a qualitative change of the considered equipment components (i.e., heat exchangers, expander, pump) and would be outside the scope of the present work, which is oriented toward smaller system scales.

4.3. Comparison of Results to Relevant Studies

In order to properly establish the undertaken optimization procedure, a comparison to similar analyses is carried out. In particular, techno-economic studies oriented towards small-to-medium scale (below 2 MW$_e$ [90]), exclusively solar-driven, medium-to-high temperature (above 150 °C) ORC systems are taken as reference. The summary of the non-exhaustive comparison is reported in Table 13, where LCoE values are converted to 2020 equivalent values accounting for inflation rates. It is also stressed that in these studies, similar climates in terms of solar irradiance were investigated, thus neglecting the effect of climate on the results.

Table 13. Comparison summary between present work and related studies.

Reference	System Type	Heat Source Temperature (°C)	Design Power Capacity (kW)	LCoE (€2020/kWh)
Current study	PTC w/TES	180–210	6.2	0.343
[92]	LFC w/TES	210–280	2.0	4.719
[26]	PTC w/TES	275	50.0	0.171
[91]	LFC w/o TES	210	171.8	0.045
[94]	LFC w/o TES	275	700.0	0.177
[94]	LFC w/TES	275	700.0	0.120
[93]	Polymer-foil CSP w/TES	165–300	1000.0	0.141
[93]	Polymer-foil CSP w/TES	165–300	1000.0	0.163
[95]	PTC w/TES	300	1000.0	0.200
[90]	PTC w/o TES	250	1000.0	0.301

As shown, the hereby obtained LCoE (0.343 €/kWh) is higher than most of the others, yet within an acceptable range. First and foremost, it is apparent that economies of scale exist, leading to substantially lower cost of energy in medium-scale systems. In addition, this cost discrepancy is further explained by the different system layouts and operation, as well as the conditions (heat source and heat sink temperature, power range) and assumptions made, such as the economic terms (years of evaluation and discount ratio) and the simulation strategy. Namely, the very low LCoE reported by Sun et al. [91] is mainly attributed to the overestimation of ORC efficiency (15.26%) and the assumption of constant-efficiency ORC operation throughout the evaluation period. On the other hand, the very high LCoE presented in the study of Ciocolanti et al. [92] is expected, as it refers to a very small-scale prototype which, additionally, is intended for CHP operation and, as a result, a large amount of the available heat is utilized for heating purposes.

Moreover, the comparative works of Desai et al. [93] and Petrollesse and Cocco [94] highlight the importance of TES in the economic feasibility of such systems thanks to the increased operating time. In this context, as shown in the 1 MWe system of Desai and Bandyopadhyay [90], the operation without TES diminishes the positive effect of economies of scale resulting in similar cost with systems of lower capacity. Ultimately, the 50 kWe system proposed by Patil et al. [26] attained a low LCoE thanks to the combination of increased system's capacity factor (0.56) and low storage cost.

Concluding, the reported cost has derived from an optimization analysis of a system incorporating TES using detailed off-design modeling to properly estimate the net produced electricity. Furthermore, present cost values were included covering all types of the system cost. Hence, it appears that the achieved LCoE is acceptable and could be further reduced in a larger-scale application.

5. Conclusions

In this study, a techno-economic optimization methodology of a small-scale medium-to-high-temperature solar ORC was presented The system was optimized using a genetic

algorithm to maximize the total annual energy efficiency and minimize the LCoE for five European cities accounting for several working fluids and two types of concentrating collectors, PTCs and PDCs. The main conclusions of the study are summarized below:

- The use of concentrating collectors (PTC and PDC) requires the integration of a sun tracking system, which increases the total solar irradiance absorbed by the collectors, by roughly 7.5% on an annual basis.
- Although there are no great differences in the energy efficiency between the systems that use different types of collectors, in most cases systems using PDCs perform slightly better. However, regarding cost-effectiveness, PTCs are more profitable from an economic perspective due to their lower purchase costs.
- The selection of the working fluid is strongly correlated to the temperature of the heat source. The optimal performance is achieved in most cases by working fluids with critical temperature slightly higher than the cycle's top temperature. In the examined system with a driving temperature between 180–210 °C, Cyclopentane and Cyclohexane give the optimal results.
- The maximum total annual solar conversion efficiency of the systems was around 10.5–11%. The best results were obtained for northern locations (e.g., Brussels) and lower values of the collecting surface, as they enabled the operation of the ORC closer to its design point for longer periods.
- On the other hand, the cost of the produced electrical energy was lower for southern locations (e.g., Athens with 0.34 €/kWh) with higher values of the collecting surface and low storage tank capacities. However, its minimum value was found to be at least around 1.5 times higher than the current commercial cost of electricity.
- An improvement of the economic performance of the system can be achieved by increasing its power production. Namely, a 6% decrease in LCoE in the case of Athens with PTC and cyclopentane as a working fluid can be attained.
- Higher LCoE values were reported compared to relevant literature studies, owing to the small-scale of the system along with the efficiency deterioration in off-design operation that was taken into account in the employed component models.

Nomenclature

A	Surface	(m^2)
Bo	Boiling number	(-)
C	Component cost	(€)
CAPEX	Capital investment expenses	(€)
D	Diameter	(m)
f	Friction factor	(-)
ff	Filling factor	(-)
h	Enthalpy	(J kg^{-1})
i	Discount rate	(-)
I$_{sol}$	Solar irradiance	(W m^{-2})
L	Length	(m)
LCoE	Levelized cost of electricity	(€ kWh^{-1})
L$_p$	vertical plate length	(m)
M	Total mass	(kg)
$\dot{m}$	Mass flow rate	(kg s^{-1})
N	Rotational speed	(rpm)
n	Investment lifetime	(years)
Nu	Nusselt number	(-)
OPEX	Annual operational expenses	(€)
r$_P$	Pressure ratio	(-)
$\dot{Q}$	Heat	flux
Re	Reynolds number	(-)
T	Temperature	(K)
t	Time	(s)
U$_l$	Heat losses coefficient	(W m^{-2} K^{-1})
$\dot{W}$	Power	(W)
$\dot{W}_{mech}$	Mechanical power	(W)
V	Volume	(m^3)
V$_s$	Displacement volume of expander	(m^3)
$\dot{V}$	volumetric flowrate	(m^3 s^{-1})
v	velocity	(m s^{-1})

Greek symbols

Δp	pressure difference	(bar)
Λ	Corrugation pitch	(m)
λ	Thermal conductivity	(W m^{-1} K^{-1})
η	Efficiency	(–)
ϱ	Density	(kg m^{-3})
φ	Chevron angle	(deg)

Subscript

amb	Ambient
ch	Channel
col	Collectors
cond	Condenser
crit	Critical
el	Electrical
eq	Equivalent
evap	Evaporator
exp	Expander
gen	Generator (expander's)
h	Hydraulic

hex   Heat exchanger
HTF   Heat transfer fluid
i   Inlet
inv   Inverter
ins   Installation
iorc   Intermediate ORC circuit
is   Isentropic
L   Referring to saturated liquid conditions
misc   Miscellaneous
motor   Pump's motor
net   Net (referring to the power)
nom   Nominal
o   Outlet
orc   Referring to the ORC subsystem
pump   Referring to the pump
pip   Pipeline
rec   Recuperator
rt   Receiver tank
sol   Solar
st   Storage
th   Thermal
tot   Total

Abbreviations

CCHP   combined cooling heat and power
CFD   computational fluid dynamics
CHP   combined heat and power
CSP   concentrated solar power
ETC   evacuated tube collectors
FPC   flat plate collectors
GA   genetic algorithm
HTF   heat transfer fluid
LFC   linear Fresnel collectors
ORC   Organic Rankine Cycle
PDC   parabolic dish collectors
PTC   parabolic trough collectors
PV   photovoltaic
RES   renewable energy sources
TES   thermal energy storage
VCC   vapor compression cycle

Appendix A

Modeling Strategies

The implementation of the solar subsystem model is based on the independent operation of the collectors' loop and the intermediate heat transfer loop, both of which are coupled or decoupled from the ORC depending on the prevailing conditions, as shown in the flow chart of Figure A1. In particular, at any given hour, the ORC is operational when the accumulated heat in the storage tank is greater than the minimum heat required for its operation.
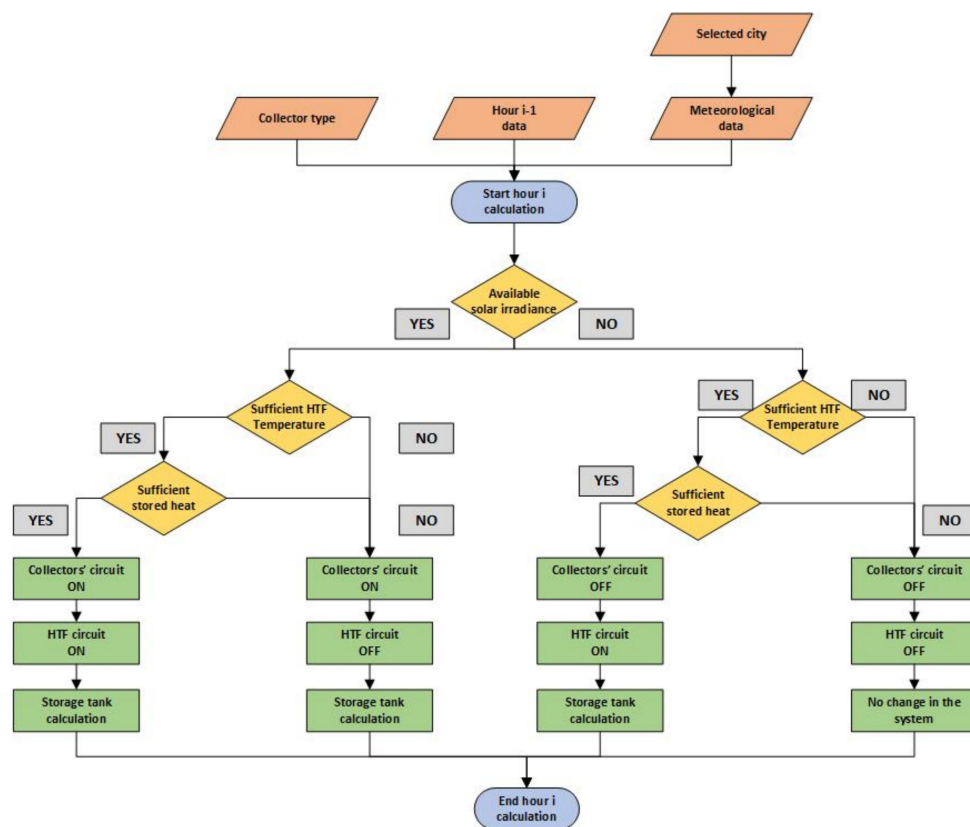
Figure A1. Flowchart of the solar subsystem modeling procedure.

In Figure A2, the on-design procedure for the ORC circuit which leads to the final sizing of its components is illustrated. For dry working fluids, the evaporation and condensing temperatures are defined based on the HTF and cooling water temperatures at the evaporator and condenser inlet and the selected pinch point values in these heat exchangers. For wet working fluids, the minimum superheating that leads to a single-phase state at the expander's output is selected.

Regarding the off-design modeling of the ORC, for each time step, the evaporation and condensation pressures are calculated by applying a 5 K and 10 K pinch point requirement in the evaporator and condenser, respectively. Regarding the expanders, three scenarios are discerned. For pressure ratios lower than the maximum value, a single expander is utilized, while for higher values two serial expanders are operational with the same pressure ratio. At the same time, their rotational speeds are regulated to achieve their gradual insertion into the system until they reach the maximum power load.

Based on the data deriving from the aforementioned analysis, the solar and the ORC sub-systems can be coupled to model the operation of the overall system for each hour step within an annual period. As shown in Figure A3, at each time step, the solar loop is operational when there is sufficient direct solar irradiance, in which case heat absorbed from the collectors is transferred to the storage tank. When there is no solar irradiance, the collectors are decoupled from the storage tank.

Regarding the ORC, its operation status depends on the temperature of the tank's top zone, as well as on the availability of stored heat. When the temperature of the tank's top zone is higher than the threshold temperature (T_{thr}) and the stored heat in the tank is sufficient, the HTF flows towards the evaporator heating the working fluid. Depending on the driving temperature, a polynomial fitting on the off-design data is performed and the cycle's output parameters are derived. If the temperature of the tank's top zone is lower or the stored heat is insufficient, the ORC loop is deactivated with no heat transferred to the evaporator.
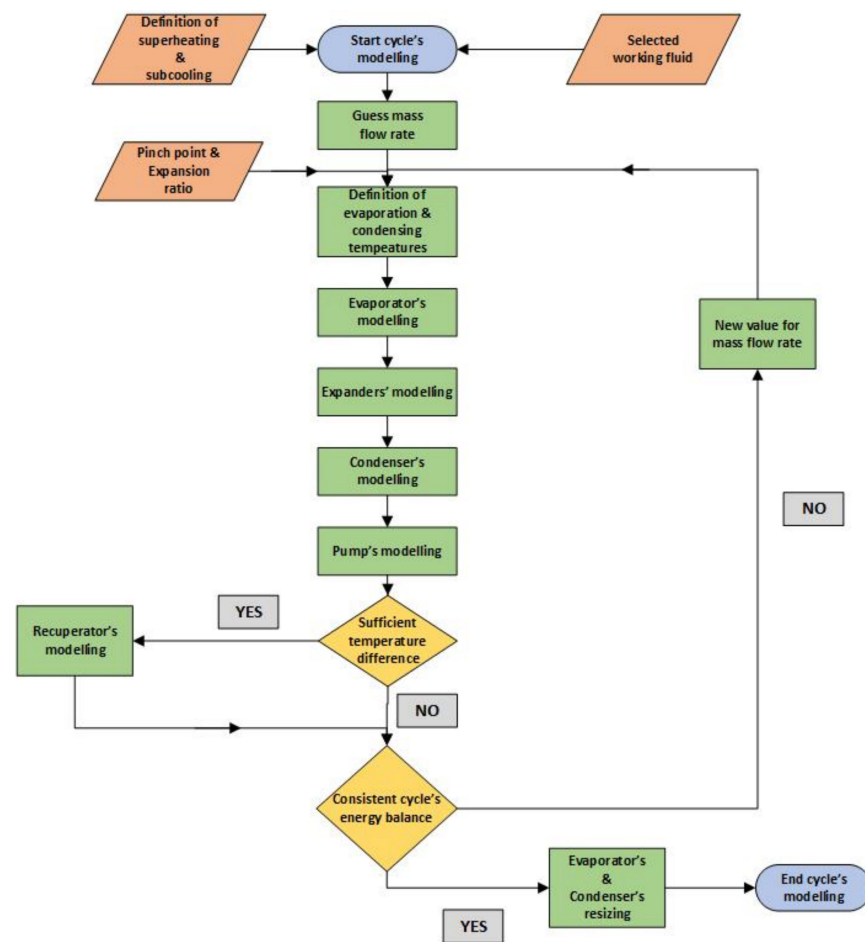
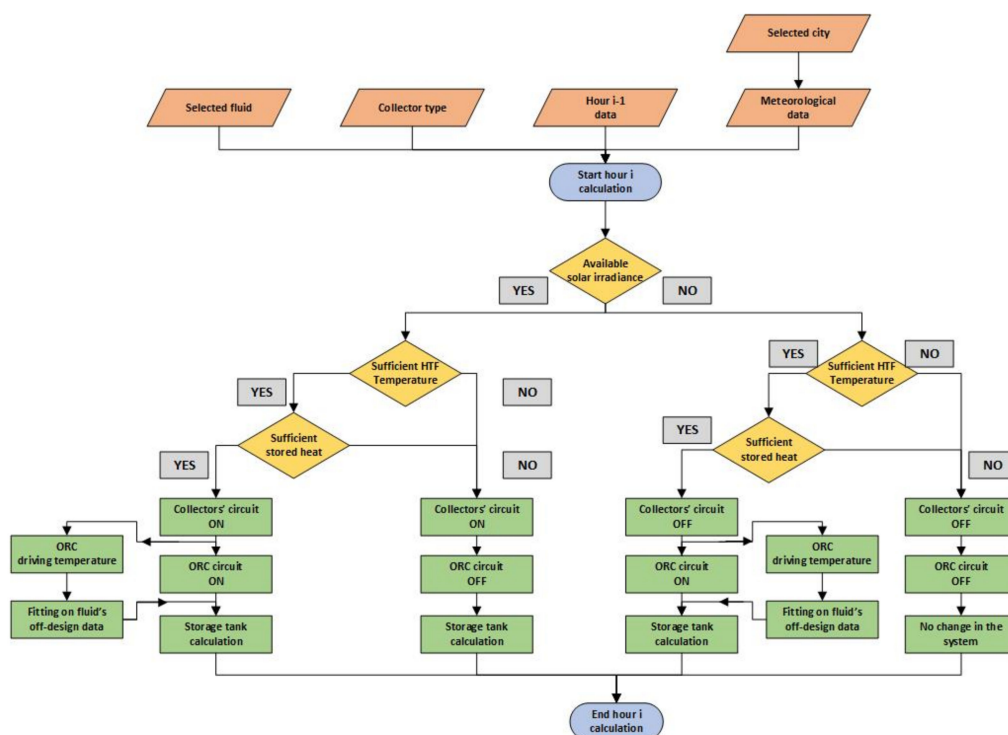**Figure A2.** Flowchart of the ORC on-design modeling procedure.

Figure A3. Flowchart of the overall system off-design modeling procedure.

References

1. Zanellato, L.; Astolfi, M.; Serafino, A.; Rizzi, D.; Macchi, E. Field Performance Evaluation of ORC Geothermal Power Plants Using Radial Outflow Turbines. *Energy Procedia* **2017**, *129*, 607–614. [CrossRef]
2. Świerzewski, M.; Kalina, J. Optimisation of biomass-fired cogeneration plants using ORC technology. *Renew. Energy* **2020**, *159*, 195–214. [CrossRef]
3. Georgousopoulos, S.; Braimakis, K.; Grimekis, D.; Karellas, S. Thermodynamic and techno-economic assessment of pure and zeotropic fluid ORCs for waste heat recovery in a biomass IGCC plant. *Appl. Therm. Eng.* **2021**, *183*, 116202. [CrossRef]
4. Karellas, S.; Braimakis, K. Energy–exergy analysis and economic investigation of a cogeneration and trigeneration ORC–VCC hybrid system utilizing biomass fuel and solar power. *Energy Convers. Manag.* **2016**, *107*, 103–113. [CrossRef]
5. Delgado-Torres, A.M.; García-Rodríguez, L. Design recommendations for solar organic Rankine cycle (ORC)–powered reverse osmosis (RO) desalination. *Renew. Sustain. Energy Rev.* **2012**, *16*, 44–53. [CrossRef]
6. Mohammed Wazed, S.; Hughes, B.R.; O'Connor, D.; Kaiser Calautit, J. A review of sustainable solar irrigation systems for Sub-Saharan Africa. *Renew. Sustain. Energy Rev.* **2018**, *81*, 1206–1225. [CrossRef]
7. Orosz, M.; Dickes, R. 16-Solar thermal powered Organic Rankine Cycles. In *Organic Rankine Cycle (ORC) Power Systems*; Macchi, E., Astolfi, M., Eds.; Woodhead Publishing: Cambridge, UK, 2017; pp. 569–612. [CrossRef]
8. Tchanche, B.F.; Papadakis, G.; Lambrinos, G.; Frangoudakis, A. Fluid selection for a low-temperature solar organic Rankine cycle. *Appl. Therm. Eng.* **2009**, *29*, 2468–2476. [CrossRef]
9. Delgado-Torres, A.M.; García-Rodríguez, L. Analysis and optimization of the low-temperature solar organic Rankine cycle (ORC). *Energy Convers. Manag.* **2010**, *51*, 2846–2856. [CrossRef]
10. Ferrara, F.; Gimelli, A.; Luongo, A. Small-scale Concentrated Solar Power (CSP) Plant: ORCs Comparison for Different Organic Fluids. *Energy Procedia* **2014**, *45*, 217–226. [CrossRef]
11. Shahverdi, K.; Loni, R.; Ghobadian, B.; Monem, M.J.; Gohari, S.; Marofi, S.; Najafi, G. Energy harvesting using solar ORC system and Archimedes Screw Turbine (AST) combination with different refrigerant working fluids. *Energy Convers. Manag.* **2019**, *187*, 205–220. [CrossRef]
12. Deligant, M.; Sauret, E.; Danel, Q.; Bakir, F. Performance assessment of a standard radial turbine as turbo expander for an adapted solar concentration ORC. *Renew. Energy* **2020**, *147*, 2833–2841. [CrossRef]
13. Toujani, N.; Bouaziz, N.; Chrigui, M.; Kairouani, L. The Impact of Operating Parameters on the Performance of a New ORC–VCC Combination for Cogeneration. *Therm. Eng.* **2020**, *67*, 660–672. [CrossRef]
14. Cioccolanti, L.; Villarini, M.; Tascioni, R.; Bocci, E. Performance assessment of a solar trigeneration system for residential applications by means of a modelling study. *Energy Procedia* **2017**, *126*, 445–452. [CrossRef]
15. Roumpedakis, T.C.; Christou, T.; Monokrousou, E.; Braimakis, K.; Karellas, S. Integrated ORC-Adsorption cycle: A first and second law analysis of potential configurations. *Energy* **2019**, *179*, 46–58. [CrossRef]
16. Braimakis, K. Solar ejector cooling systems: A review. *Renew. Energy* **2021**, *164*, 566–602. [CrossRef]
17. Jafary, S.; Khalilarya, S.; Shawabkeh, A.; Wae-hayee, M.; Hashemian, M. A complete energetic and exergetic analysis of a solar powered trigeneration system with two novel organic Rankine cycle (ORC) configurations. *J. Clean. Prod.* **2021**, *281*, 124552. [CrossRef]
18. Khaliq, A.; Mokheimer, E.M.A.; Yaqub, M. Thermodynamic investigations on a novel solar powered trigeneration energy system. *Energy Convers. Manag.* **2019**, *188*, 398–413. [CrossRef]
19. Braimakis, K.; Thimo, A.; Karellas, S. Technoeconomic Analysis and Comparison of a Solar-Based Biomass ORC-VCC System and a PV Heat Pump for Domestic Trigeneration. *J. Energy Eng.* **2017**, *143*, 04016048. [CrossRef]
20. Baccioli, A.; Antonelli, M.; Desideri, U. Dynamic modeling of a solar ORC with compound parabolic collectors: Annual production and comparison with steady-state simulation. *Energy Convers. Manag.* **2017**, *148*, 708–723. [CrossRef]
21. Wang, M.; Wang, J.; Zhao, Y.; Zhao, P.; Dai, Y. Thermodynamic analysis and optimization of a solar-driven regenerative organic Rankine cycle (ORC) based on flat-plate solar collectors. *Appl. Therm. Eng.* **2013**, *50*, 816–825. [CrossRef]
22. Freeman, J.; Hellgardt, K.; Markides, C.N. Working fluid selection and electrical performance optimisation of a domestic solar-ORC combined heat and power system for year-round operation in the UK. *Appl. Energy* **2017**, *186*, 291–303. [CrossRef]
23. Kutlu, C.; Li, J.; Su, Y.; Pei, G.; Riffat, S. Off-design performance modelling of a solar organic Rankine cycle integrated with pressurized hot water storage unit for community level application. *Energy Convers. Manag.* **2018**, *166*, 132–145. [CrossRef]
24. Petrollese, M.; Cocco, D. Robust optimization for the preliminary design of solar organic Rankine cycle (ORC) systems. *Energy Convers. Manag.* **2019**, *184*, 338–349. [CrossRef]
25. Casartelli, D.; Binotti, M.; Silva, P.; Macchi, E.; Roccaro, E.; Passera, T. Power Block Off-design Control Strategies for Indirect Solar ORC Cycles. *Energy Procedia* **2015**, *69*, 1220–1230. [CrossRef]
26. Patil, V.R.; Biradar, V.I.; Shreyas, R.; Garg, P.; Orosz, M.S.; Thirumalai, N.C. Techno-economic comparison of solar organic Rankine cycle (ORC) and photovoltaic (PV) systems with energy storage. *Renew. Energy* **2017**, *113*, 1250–1260. [CrossRef]
27. Li, S.; Ma, H.; Li, W. Dynamic performance analysis of solar organic Rankine cycle with thermal energy storage. *Appl. Therm. Eng.* **2018**, *129*, 155–164. [CrossRef]
28. Peel, M.C.; Finlayson, B.L.; McMahon, T.A. Updated world map of the Köppen-Geiger climate classification. *Hydrol. Earth Syst. Sci.* **2007**, *11*, 1633–1644. [CrossRef]

29. Imran, M.; Usman, M.; Park, B.-S.; Kim, H.-J.; Lee, D.-H. Multi-objective optimization of evaporator of organic Rankine cycle (ORC) for low temperature geothermal heat source. *Appl. Therm. Eng.* **2015**, *80*, 1–9. [CrossRef]

30. Xi, H.; Li, M.-J.; Xu, C.; He, Y.-L. Parametric optimization of regenerative organic Rankine cycle (ORC) for low grade waste heat recovery using genetic algorithm. *Energy* **2013**, *58*, 473–482. [CrossRef]

31. Bekiloğlu, H.E.; Bedir, H.; Anlaş, G. Multi-objective optimization of ORC parameters and selection of working fluid using preliminary radial inflow turbine design. *Energy Convers. Manag.* **2019**, *183*, 833–847. [CrossRef]

32. Jankowski, M.; Borsukiewicz, A. Multi-objective approach for determination of optimal operating parameters in low-temperature ORC power plant. *Energy Convers. Manag.* **2019**, *200*, 112075. [CrossRef]

33. Zhu, G.; Wendelin, T.; Wagner, M.J.; Kutscher, C. History, current state, and future of linear Fresnel concentrating solar collectors. *Sol. Energy* **2014**, *103*, 639–652. [CrossRef]

34. Suman, S.; Khan, M.K.; Pathak, M. Performance enhancement of solar collectors—A review. *Renew. Sustain. Energy Rev.* **2015**, *49*, 192–210. [CrossRef]

35. Infante Ferreira, C.; Kim, D.-S. Techno-economic review of solar cooling technologies based on location-specific data. *Int. J. Refrig.* **2014**, *39*, 23–37. [CrossRef]

36. Kasaeian, A.; Daviran, S.; Azarian, R.D.; Rashidi, A. Performance evaluation and nanofluid using capability study of a solar parabolic trough collector. *Energy Convers. Manag.* **2015**, *89*, 368–375. [CrossRef]

37. Loni, R.; Kasaeian, A.; Asli-Ardeh, E.A.; Ghobadian, B.; Gorjian, S. Experimental and numerical study on dish concentrator with cubical and cylindrical cavity receivers using thermal oil. *Energy* **2018**, *154*, 168–181. [CrossRef]

38. Duffie, J.A.; Beckman, W.A.; Worek, W. *Solar Engineering of Thermal Processes*; Wiley Online Library: Hoboken, NJ, USA, 2013; Volume 3.

39. Wischhusen, S. An enhanced discretization method for storage tank models within energy systems. In Proceedings of the 5th International Modelica Conference, Vienna, Austria, 4–5 September 2006; pp. 243–248.

40. Roumpedakis, T. *Techo-Economic Investigations of a Solar Driven ORC-Sorption System for Combined Cooling, Heating and Power*; TU Delft: Delft, The Netherlands, 2018.

41. Raccanello, J.; Rech, S.; Lazzaretto, A. Simplified dynamic modeling of single-tank thermal energy storage systems. *Energy* **2019**, *182*, 1154–1172. [CrossRef]

42. Bellos, E.; Tzivanidis, C.; Antonopoulos, K.A. Exergetic, energetic and financial evaluation of a solar driven absorption cooling system with various collector types. *Appl. Therm. Eng.* **2016**, *102*, 749–759. [CrossRef]

43. Abed, N.; Afgan, I.; Cioncolini, A.; Iacovides, H.; Nasser, A. Assessment and evaluation of the thermal performance of various working fluids in parabolic trough collectors of solar thermal power plants under non-uniform heat flux distribution conditions. *Energies* **2020**, *13*, 3776. [CrossRef]

44. Karellas, S.; Roumpedakis, T.C. Chapter 7—Solar thermal power plants. In *Solar Hydrogen Production*; Calise, F., D'Accadia, M.D., Santarelli, M., Lanzini, A., Ferrero, D., Eds.; Academic Press: Amsterdam, The Netherlands, 2019; pp. 179–235. [CrossRef]

45. VDI Gesellschaft Verfahrenstechnik und Chemieingenieurwesen. *VDI Heat Atlas*, 2nd ed.; Springer: Berlin/Heidelberg, Germany, 2010.

46. Yan, Y.-Y.; Lin, T.-F. Evaporation heat transfer and pressure drop of refrigerant R-134a in a plate heat exchanger. *J. Heat Transf.* **1999**, *121*, 118–127. [CrossRef]

47. Focke, W.; Zachariades, J.; Olivier, I. The effect of the corrugation inclination angle on the thermohydraulic performance of plate heat exchangers. *Int. J. Heat Mass Transf.* **1985**, *28*, 1469–1479. [CrossRef]

48. Hsieh, Y.Y.; Lin, T.F. Saturated flow boiling heat transfer and pressure drop of refrigerant R-410A in a vertical plate heat exchanger. *Int. J. Heat Mass Transf.* **2002**, *45*, 1033–1044. [CrossRef]

49. Thonon, B.; Bontemps, A. Condensation of pure and mixture of hydrocarbons in a compact heat exchanger: Experiments and modelling. *Heat Transf. Eng.* **2002**, *23*, 3–17. [CrossRef]

50. Han, D.-H.; Lee, K.-J.; Kim, Y.-H. The characteristics of condensation in brazed plate heat exchangers with different chevron angles. *J. Korean Phys. Soc.* **2003**, *43*, 66–73.

51. Donowski, V.D.; Kandlikar, S.G. Correlating evaporation heat transfer coefficient of refrigerant R-134a in a plate heat exchanger. In Proceedings of the Engineering Foundation Conference on Pool and Flow Boiling, Anchorage, AK, USA, 30 April–5 May 2000; pp. 1–18.

52. Thonon, B.; Vidil, R.; Marvillet, C. Recent research and developments in plate heat exchangers. *J. Enhanc. Heat Transf.* **1995**, *2*, 149–155. [CrossRef]

53. Wanner_Engineering_Hydra_Cell. Hydra Cell Pumps G25 Series. Available online: https://www.hydra-cell.co.uk/docs/Sales-Lit-Extranet-Datasheets/G25-Datasheet.pdf (accessed on 13 May 2021).

54. Ziviani, D.; Gusev, S.; Lecompte, S.; Groll, E.; Braun, J.; Horton, W.T.; van den Broek, M.; De Paepe, M. Characterizing the performance of a single-screw expander in a small-scale organic Rankine cycle for waste heat recovery. *Appl. Energy* **2016**, *181*, 155–170. [CrossRef]

55. Roumpedakis, T.C.; Loumpardis, G.; Karellas, S. Exergetic and Economic Analysis of a Solar Driven Small Scale ORC. In Proceedings of the ORC2019, Athens, Greece, 9–11 September 2019.

56. Hsu, S.-W.; Chiang, H.-W.; Yen, C.-W. Experimental investigation of the performance of a hermetic screw-expander organic Rankine cycle. *Energies* **2014**, *7*, 6172–6185. [CrossRef]

57. Quoilin, S.; Broek, M.V.D.; Declaye, S.; Dewallef, P.; Lemort, V. Techno-economic survey of Organic Rankine Cycle (ORC) systems. *Renew. Sustain. Energy Rev.* **2013**, *22*, 168–186. [CrossRef]

58. Wang, W.; Shen, L.-L.; Chen, R.-M.; Wu, Y.-T.; Ma, C.-F. Experimental Study on Heat Loss of a Single Screw Expander for an Organic Rankine Cycle System. *Front. Energy Res.* **2020**, *8*, 1–10. [CrossRef]

59. Lemort, V.; Quoilin, S.; Cuevas, C.; Lebrun, J. Testing and modeling a scroll expander integrated into an Organic Rankine Cycle. *Appl. Therm. Eng.* **2009**, *29*, 3094–3102. [CrossRef]

60. Giuffrida, A. Improving the semi-empirical modelling of a single-screw expander for small organic Rankine cycles. *Appl. Energy* **2017**, *193*, 356–368. [CrossRef]

61. Dumont, O.; Dickes, R.; Lemort, V. Experimental investigation of four volumetric expanders. *Energy Procedia* **2017**, *129*, 859–866. [CrossRef]

62. Quoilin, S.; Declaye, S.; Tchanche, B.F.; Lemort, V. Thermo-economic optimization of waste heat recovery Organic Rankine Cycles. *Appl. Therm. Eng.* **2011**, *31*, 2885–2893. [CrossRef]

63. Bao, J.; Zhao, L. A review of working fluid and expander selections for organic Rankine cycle. *Renew. Sustain. Energy Rev.* **2013**, *24*, 325–342. [CrossRef]

64. Braimakis, K.; Karellas, S. Energetic optimization of regenerative Organic Rankine Cycle (ORC) configurations. *Energy Convers. Manag.* **2018**, *159*, 353–370. [CrossRef]

65. Maraver, D.; Uche, J.; Royo, J. Assessment of high temperature organic Rankine cycle engine for polygeneration with MED desalination: A preliminary approach. *Energy Convers. Manag.* **2012**, *53*, 108–117. [CrossRef]

66. Braimakis, K.; Roumpedakis, T.C.; Leontaritis, A.-D.; Karellas, S. Comparison of Environmentally Friendly Working Fluids for Organic Rankine Cycles. In *Advances in New Heat Transfer Fluids: From Numerical to Experimental Techniques*; Minea, A.A., Ed.; CRC Press: Boca Raton, FL, USA, 2016; pp. 377–426.

67. Kurup, P.; Turchi, C. *Parabolic Trough Collector Cost Update for the System Advisor Model (SAM)*; National Renewable Energy Laboratory: Denver, CO, USA, 2015. [CrossRef]

68. Mancini, T.; Heller, P.; Butler, B.; Osborn, B.; Schiel, W.; Goldberg, V.; Buck, R.; Diver, R.; Andraka, C.; Moreno, J. Dish-Stirling systems: An overview of development and status. *J. Sol. Energy Eng.* **2003**, *125*, 135–151. [CrossRef]

69. Poullikkas, A.; Kourtis, G.; Hadjipaschalis, I. Parametric analysis for the installation of solar dish technologies in Mediterranean regions. *Renew. Sustain. Energy Rev.* **2010**, *14*, 2772–2783. [CrossRef]

70. Lecompte, S.; Huisseune, H.; van den Broek, M.; De Schampheleire, S.; De Paepe, M. Part load based thermo-economic optimization of the Organic Rankine Cycle (ORC) applied to a combined heat and power (CHP) system. *Appl. Energy* **2013**, *111*, 871–881. [CrossRef]

71. Zilmet USA. *Zilmet USA List Price Catalog*; Zilmet USA: East Greenwich, RI, USA, 2016.

72. Boyaghchi, F.A.; Heidarnejad, P. Thermoeconomic assessment and multi objective optimization of a solar micro CCHP based on Organic Rankine Cycle for domestic application. *Energy Convers. Manag.* **2015**, *97*, 224–234. [CrossRef]

73. Astolfi, M. *An Innovative Approach for the Techno-Economic Optimization of Organic Rankine Cycles*; Politecnico di Milano: Milan, Italy, 2014.

74. Zauba_Technologies. Import & Export Data. Available online: https://www.zauba.com/importanalysis-cyclopentane-report.html (accessed on 13 May 2021).

75. Zauba_Technologies. Import & Export Data. Available online: https://www.zauba.com/importanalysis-cyclohexane-report.html (accessed on 13 May 2021).

76. Zauba_Technologies. Import & Export Data. Available online: https://www.zauba.com/importanalysis-isohexane-report.html (accessed on 13 May 2021).

77. Zauba_Technologies. Import & Export Data. Available online: https://www.zauba.com/importanalysis-hexane-report.html (accessed on 13 May 2021).

78. Zauba_Technologies. Import & Export Data. Available online: https://www.zauba.com/importanalysis-benzene-report.html (accessed on 13 May 2021).

79. Zauba_Technologies. Import & Export Data. Available online: https://www.zauba.com/importanalysis-toluene-report.html (accessed on 13 May 2021).

80. Zauba_Technologies. Import & Export Data. Available online: https://www.zauba.com/importanalysis-therminol-vp-1-report.html (accessed on 13 May 2021).

81. Pallis, P. *Experimental Investigation and Economic Assessment of a Fully Automated ORC for Waste Heat Recovery from Marine Engine Jacket Cooling Water*; National Technical University of Athens: Athens, Greece, 2020.

82. Leontaritis, A.-D.; Pallis, P.; Karellas, S.; Papastergiou, A.; Antoniou, N.; Vourliotis, P.; Kakalis, N.M.; Dimopoulos, G. Experimental study on a low temperature ORC unit for onboard waste heat recovery from marine diesel engines. In Proceedings of the 3rd International Seminar on ORC Power Systems, Brussels, Belgium, 12–14 October 2015; p. 1.

83. Roumpedakis, T.C.; Chapaloglou, S.; Pallis, P.; Leontaritis, A.-D.; Braimakis, K.; Karellas, S.; Vourliotis, P. Experimental Investigation and CFD Analysis of Heat Transfer in Single Phase Subcooler of a Small Scale Waste Heat Recovery ORC. *Energy Procedia* **2017**, *129*, 487–494. [CrossRef]

84. Ueckerdt, F.; Hirth, L.; Luderer, G.; Edenhofer, O. System LCOE: What are the costs of variable renewables? *Energy* **2013**, *63*, 61–75. [CrossRef]

85. Eurostat. Electricity Prices, Second Half of Year. 2020. Available online: https://ec.europa.eu/eurostat/statistics-explained/index.php/Electricity_price_statistics (accessed on 15 April 2021).

86. European Parliament. Council of the European Union. Directive (EU) 2018/2001 of the European Parliament and of the Council of 11 December 2018 on the promotion of the use of energy from renewable sources. *Off. J. Eur. Union* **2018**, 82–209. Available online: http://data.europa.eu/eli/dir/2018/2001/oj (accessed on 11 December 2018).

87. Roumpedakis, T.C.; Kallis, G.; Magiri-Skouloudi, D.; Grimekis, D.; Karellas, S. Life cycle analysis of ZEOSOL solar cooling and heating system. *Renew. Energy* **2020**, *154*, 82–98. [CrossRef]

88. Deb, K.; Pratap, A.; Agarwal, S.; Meyarivan, T. A fast and elitist multiobjective genetic algorithm: NSGA-II. *IEEE Trans. Evol. Comput.* **2002**, *6*, 182–197. [CrossRef]

89. Bódis, K.; Kougias, I.; Jäger-Waldau, A.; Taylor, N.; Szabó, S. A high-resolution geospatial assessment of the rooftop solar photovoltaic potential in the European Union. *Renew. Sustain. Energy Rev.* **2019**, *114*, 109309. [CrossRef]

90. Desai, N.B.; Bandyopadhyay, S. Thermo-economic analysis and selection of working fluid for solar organic Rankine cycle. *Appl. Therm. Eng.* **2016**, *95*, 471–481. [CrossRef]

91. Sun, K.; Zhao, T.; Wu, S.; Yang, S. Comprehensive evaluation of concentrated solar collector and Organic Rankine cycle hybrid energy process with considering the effects of different heat transfer fluids. *Energy Rep.* **2021**, *7*, 362–384. [CrossRef]

92. Cioccolanti, L.; Tascioni, R.; Arteconi, A. Mathematical modelling of operation modes and performance evaluation of an innovative small-scale concentrated solar organic Rankine cycle plant. *Appl. Energy* **2018**, *221*, 464–476. [CrossRef]

93. Desai, N.B.; Pranov, H.; Haglind, F. Techno-economic analysis of a foil-based solar collector driven electricity and fresh water generation system. *Renew. Energy* **2021**, *165*, 642–656. [CrossRef]

94. Petrollese, M.; Cocco, D. A multi-scenario approach for a robust design of solar-based ORC systems. *Renew. Energy* **2020**, *161*, 1184–1194. [CrossRef]

95. El Hamdani, F.; Vaudreuil, S.; Abderafi, S.; Bounahmidi, T. Techno-Economic Evaluation of a Concentrating Solar Power Plant Driven by an Organic Rankine Cycle. *J. Sol. Energy Eng.* **2020**, *142*, 1–36. [CrossRef]